MASTER THESIS OF THE UNIVERSITÉ BOURGOGNE FRANCHE-COMTÉ, FRANCE

AND OF THE CENTRO DE INVESTIGACIONES EN ÓPTICA, MEXICO

CONDUCTED AT FEMTO-ST INSTITUTE

International MSc on Control for Green Mechatronics (GREEM)
a speciality of Control & Robotics (UBFC)

and

MSc in Optomechatronics (CIO)

Year Group: 2019

by

Julio Andrés IGLESIAS MARTÍNEZ

Contribution to the characterization of mechanical displacements and quality factors of micron-scale phononic resonators

Thesis Supervisor:

Dr Sarah BENCHABANE GAIFFE, Internship Responsible,
Chargée de recherche CNRS, FEMTO-ST Institute

Academic Advisors:

Dr Micky RAKOTONDRABE, Associate Professor with HDR, UBFC
Dr Geminiano Donaciano MARTINEZ PONCE, Investigador Titular B, CIO

UBFC INE: 05DU7T00M51 CIO student Number: DFA/A/MOPTO/354

ACKNOWLEDGEMENT

I would like to thank my thesis advisor Dr. Sarah Benchabane from the FEMTO-ST Institute . The door to Dr. Benchabane's office was always open whenever I ran into a trouble spot or had a question about my research or writing. She consistently allowed this paper to be my own work, but steered me in the right the direction whenever she thought I needed it.

My sinciere thanks to the experts who were involved in this research project: Dr. Micky Rakotondrabe, Dr. Olivier Gaiffe and Dr. Geminiano Martínez. Without their passionate participation and input, the this thesis could not have been successfully conducted.

I would also like to thank the CIO and the UBFC for the opportunity of the Dual Degree program. And to CONACyT México for the financial support.

Finally, I want to express my very profound gratitude to my wife Dulce Yocelyn. This accomplishment would not have been possible without her support and continuous encouragement. Nothing could have been possible without her.

Thank you.

Julio Andrés IGLESIAS MARTÍNEZ

August 2019

CONTENTS

1

General Introduction

The microelectromechanical systems (MEMS) are an important contribution to the innovation of the technology that we use everyday. MEMS are attractive because of their considerable small size, low power consumption and inexpensive cost.

The characterization of MEMS is needed to develop a better performance of the device. The aim of the collected data is to corroborate that the device is working as it is supposed to, also, it offers valuable information for future designs.

MEMS devices are composed of electrical and mechanical components that form integrated electro-mechanical systems. It is important to differentiate between electrical and mechanical effects while characterizing and troubleshooting these devices. The coupled electro-mechanical behavior as well as the fabrication processes and the material conditions complicate the determination of the dynamic response of these devices.

MEMS devices are utilized because of their high quality factor. There are many types of MEMS, one of these are the Surface Acoustic Waves (SAW) devices, they are a striking example of ubiquity of MEMS in our daily lives as they are the core of mobile communication systems. This SAW devices are used as resonators, filters and sensor, are ideal thanks to their small size and high frequency responce.

The development of strategies to control SAW counts among the activities of a part of the Phononics & Microscopy research group of the MN2S department of FEMTO ST, where I did my internship that lasted six months as a part of a Dual Degree Program between the Université Bourgogne Franche-Comté and the Centro de Investigaciones en Óptica where I belong.

One of the research group's main interest is in Phononic cristals and acoustic metama-

terials over a wide range of scale and frequencies. Usually in the point of view of the materials that host this propagation such phononic crystals or acoustic metamaterials. The applications are found in vibration isolation, sound insulation, MEMS, elastic wave propagation control in RF communications, or to nanoscale thermal transport.

Aiming at application to SAW or other or other MEMS devices is demanding. Stringent conditions as high frequency, displacement nanometer or sub nanometer and microscale fingerprint have to be fulfilled. The characterization of such electro-acoustic devices is key but challenging.

The objective of the research of this thesis is to implement a homodyne Michelson interferometer that contributes to characterize the surface acoustic waves in MEMS and phononic devices. A particular focus is set in the measurement of the quality factor of mechanical resonances. There are a wide variety of measuring methods, but optical interferometry is the most suitable for frequencies in the range of GHz as well as for amplitude or the nano and picometer range [1, 2].

This report is organized as follows: In the Chapter 2, I will present the characteristics of different optical techniques designed to detect surface vibrations in micromechanical devices. Chapter 3 gives a description of the interferometrical setup developed during this internship. We will see that we have chosen to implement a Michelson Interferometer. Chapter 4 explores the implementation of the setup and illustrates its operation on a test electro-acoustic devices . Finally, the last chapter concludes the principal findings of this research.

2

Optical Detection of Mechanical Vibration

Micro and Nano electronical systems (MEMS, NEMS), are tiny devices made using the techniques of microfabrication. Their size ranges between tens of nm to thousands of μm. MEMS and NEMS take advantage of the mechanical and electrical properties of their host materials. One of the most utilized phenomenon is the generation many kinds of acoustic waves through the piezoelectric effect, such as surface acoustics waves (SAW) and bulk acoustics waves (BAW).

For SAW based devices, waves are normally generated by applying a voltage signal on a piezoelectric substrate utilizing patterned electrodes. SAWs typically have a wavelength that varies from 1 to a few lens of μm an amplitude about tens of pm and a frequency from tens of MHz to the tens of GHz.

SAW and BAW based devices are used as actuators, sensors, filters, resonators, and are a vital part of nowadays technology, for example, in the mobile phone industry. The complete characterization of MEMS is needed to optimize the design and improve the performance of the devices. The methods for its characterization must be non intrusive in order not to alter the performance of the device.

Right after the invention of the laser in the years 1960's, the first laser-based techniques were applied for the detection of acoustic waves of MEMS. This allowed to characterize the device by creating magnitude and phase maps of the vibrations, that can be obtained by scanning the measurement area point by point.

It is necessary that the measurement does not alter the integrity and the mechanical per-

formance of the device, that is why the light power density must be moderated (normally less than 20 mW). Also, it is important to choose a technique that allows to detect the smallest variation as possible; for example, a focused laser beam in the scanning setup can reach a imaging resolution limited at its best by the diffraction limit. The scanning system can be obtained in two ways: the scanning stages and the scanning mirror.

In this chapter, we will present the some of the most utilized techniques for the MEMS characterization, focusing in the optical techniques designed to detect surface vibrations in micromechanical devices.

2.1/ STATE OF ART

2.1.1/ PRINCIPLE OF AN OPTICAL DETECTION

The detection of the vibration of MEMS can be obtained by several types of methods. These are some examples of non-optical methods: Scanning Probe Microscopy, Scanning Electron Microscope and Cantilevers [3]. Using optics is relevant because of their high resolution and no contact with the structures.

Optical methods can be split into two major categories: non-interferometer based and the interferometer based. Among the techniques that do not rely on an interferometer, optical beam deflection measurement methods are probably the simplest to implement.

The knife-edge technique is an example of such methods. A laser beam is focused to the sample, then reflects to a detector. Then a knife-edge obstacle is put in the path between the sample and the photo detector in such a way that the intensity of the light observed by the detector changes if the incident angle changes.

This method is the most utilized for the in plane vibrations because of its simplicity and effectiveness, also because it is possible to combine this method with an interferometric setup, see Holmgren et al. [4]. For this method, the displacement sensitivity has been reported to be as low as $1pm/\sqrt{Hz}$, for in plane vibration and a detector limited bandwidth of 1.4 GHz [5], [6], with a band. In this case, the knife-edge obstacle is a resonator itself, see Figure 2.1.

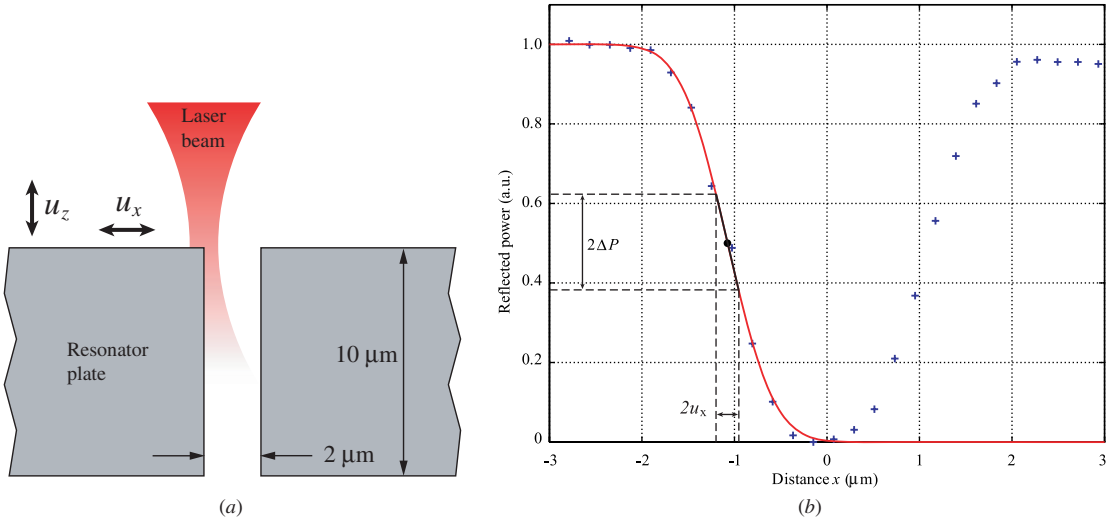

Figure 2.1: In-plane detection method: (a) cross section of an etched hole. A laser beam focused of on the sample surface. (b) Intensity profile of the laser beam reflected form the sample when the beam is scanned over an etched-hole, measurement (crosses) and fitted curve (solid line).Reproduce form [4]

For out-plane vibration, it is possible to change the knife-edge obstacle for a split or balanced photodiode and to monitor the difference between two signals that will be related to the amplitude of the vibration, as shown in Figure 2.2, [7].

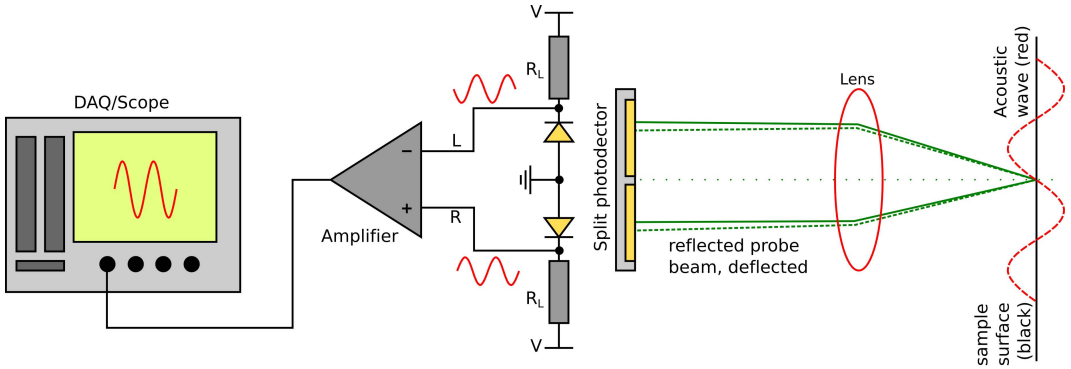

Figure 2.2: A schematic of a system that uses a knife-edge detector (KED) to detect optical deflection related with the acoustic waves, the light source is in an angle outside the paper. Reproduce from [8]

Another non-interferometer method is the diffraction grating method. In this case, the wavefront of isolation propagating on the surface of a sample works as a phase grating mask. This will diffract the beams in several orders where the angle between them is related to the wavelength of the mechanical vibration and the relative intensities of the orders are proportional to the amplitude of the vibration,[9]. This method only works for frequencies higher than 100 MHz and has low sensitivity.

One of the most recent methods is to use micro-focused surface Brillouin scattering techniques for the mapping of amplitude as recently presented by G. Carlotti [10]. This method

can be seen as a complementary to the classical surface Brillouin scattering, that it is used to perform elastic characterization in a homogeneous samples such as films [11], and is well suited for the frequency ranging between *1-500 GHz*. This method can also be used for surface acoustics waves in no-homogeneous systems such as resonators[12], due to the diffraction limited lateral resolution. The capability of this is yet to be discovered with an expected frequency response to be in the same range of the classical surface Brillouin.

The disadvantages of this method are mainly the high precision spectroscopy required to observe this scattered light and that the laser sources need to be a low narrow bandwidth and big integration time, since the amount of the scatter light is really small. 1 GHz is difficult because of the Rayleigh dispersion.

2.1.2/ VIBRATION DETECTION BY OPTICAL INTERFERENCE

An interferometer is based on the interference of two or more optical waves. Usually, one of the waves will be the reference wave and the other one interacts with the sample. Interferometers can be divided in three types: homodyne, differential and heterodyne. The interferometers can detect any kind of out of plane mechanical displacements, the origin of the vibration does not have to be specific. Rayleigh wave, Lamb wave, bulk wave or others vibration or shock can be measured by these probes.

2.1.2.1/ INTERFERENCE PRINCIPLE

Let us start with two monochromatic waves, with a wave vectors $\mathbf{k}_1$ and $\mathbf{k}_2$, the same angular frequency ω, initial phases ϕ and φ, and a amplitude $\mathbf{a}(\mathbf{r})$ and $\mathbf{b}(\mathbf{r})$.

$$\mathbf{E}(r,t) = \mathbf{a}(\mathbf{r})\cos(\mathbf{k}_1 \cdot \mathbf{r} - \omega t + \phi) \tag{2.1}$$

$$\mathbf{E}(r,t) = \mathbf{b}(\mathbf{r})\cos(\mathbf{k}_2 \cdot \mathbf{r} - \omega t + \varphi) \tag{2.2}$$

These two waves are superposed in the same position and time; the total electrical field $\mathbf{E}$, will be the sum of them thanks to the superposition principle.

$$\mathbf{E} = \mathbf{E}_1 + \mathbf{E}_2 \tag{2.3}$$

The irradiance, I, is defined as a the time average of the Poynting's vector, $\mathbf{S}$, $I = \langle \mathbf{S} \rangle$. Since the magnetic part of the wave, $\mathbf{B}$ is perpendicular to $\mathbf{E}$, the irradiance can be rewritten as, $I \propto \langle \mathbf{E}^2 \rangle$

$$\mathbf{E}^2 = (\mathbf{E}_1 + \mathbf{E}_2)^2 = \mathbf{E}_1^2 + \mathbf{E}_2^2 + 2\mathbf{E}_1 \cdot \mathbf{E}_2 \tag{2.4}$$

Now let us make the time average

$$\langle \mathbf{E}^2 \rangle = \langle \mathbf{E}_1^2 \rangle + \langle \mathbf{E}_2^2 \rangle + 2\langle \mathbf{E}_1 \cdot \mathbf{E} \rangle \tag{2.5}$$

The equation 2.5 is related to the total intensity, I. The first two terms are proportional to the total irradiance of the first wave, $I_1 \propto \langle \mathbf{E}_1^2 \rangle$, and the second wave $I_2 \propto \langle \mathbf{E}_2^2 \rangle$. The last term is called the interference term, $I_{12} \propto 2\langle \mathbf{E}_1 \cdot \mathbf{E}_2 \rangle$.

$$I = I_1 + I_2 + I_{12} \tag{2.6}$$

Let us focus on I_{12}, because the other two terms correspond to the intensity of a single wave, $\langle \mathbf{E}_1^2 \rangle = \frac{1}{2}|\mathbf{a}|^2$ and $\langle \mathbf{E}_2^2 \rangle = \frac{1}{2}|\mathbf{b}|^2$.

$$\langle \mathbf{E}_1 \cdot \mathbf{E}_2 \rangle = \langle \mathbf{a}(\mathbf{r}) \cdot \mathbf{b}(\mathbf{r}) \cos(\mathbf{k}_1 \cdot \mathbf{r} - \omega t + \phi) \cos(\mathbf{k}_2 \cdot \mathbf{r} - \omega t + \varphi) \rangle \tag{2.7}$$

Using the trigonometry relationship of $\cos(\alpha - \beta) = \cos(\alpha)\cos(\beta) + \sin(\beta)\cos(\alpha)$, we find 2.8.

$$\begin{aligned} \langle \mathbf{E}_1 \cdot \mathbf{E}_2 \rangle = \mathbf{a}(\mathbf{r}) \cdot \mathbf{b}(\mathbf{r}) \langle (\cos(\mathbf{k}_1 \cdot \mathbf{r} + \phi) \cos \omega t + \sin(\mathbf{k}_1 \cdot \mathbf{r} + \phi) \sin \omega t) \\ (\cos(\mathbf{k}_2 \cdot \mathbf{r} + \varphi) \cos \omega t + \sin(\mathbf{k}_2 \cdot \mathbf{r} + \varphi) \sin(\omega t)) \rangle \end{aligned} \tag{2.8}$$

After some algebra and noticing that the time average will only apply for the time-dependent functions,

$$\begin{aligned} \langle \mathbf{E}_1 \cdot \mathbf{E}_2 \rangle = \mathbf{a}(\mathbf{r}) \cdot \mathbf{b}(\mathbf{r}) (\cos(\mathbf{k}_1 \cdot \mathbf{r} + \phi) \cos(\mathbf{k}_2 \cdot \mathbf{r} + \varphi) \langle \cos^2 \omega t \rangle \\ + \sin(\mathbf{k}_1 \cdot \mathbf{r} + \phi) \sin(\mathbf{k}_2 \cdot \mathbf{r} + \varphi) \langle \sin^2 \omega t) \rangle \\ (\sin(\mathbf{k}_1 \cdot \mathbf{r} + \mathbf{k}_2 \cdot \mathbf{r} + \phi + \varphi) \langle \cos \omega t \sin \omega t \rangle) \end{aligned} \tag{2.9}$$

Making the time average, and assuming large integration time compared with the period of the wave, $T >> \frac{2\pi}{\omega}$, we can write $\langle \cos^2 \omega t \rangle = \frac{1}{2}$, $\langle \sin^2 \omega t \rangle = \frac{1}{2}$ and $\langle \cos \omega t \sin \omega t \rangle = 0$.

Hence, 2.9, can be simplified to 2.10, after using again trigonometric identities:

$$2\langle \mathbf{E}_1 \cdot \mathbf{E}_2 \rangle = \mathbf{a}(\mathbf{r}) \cdot \mathbf{b}(\mathbf{r})(\cos((\mathbf{k}_1 \cdot \mathbf{r} + \phi) - (\mathbf{k}_2 \cdot \mathbf{r} + \varphi))) \tag{2.10}$$

The term $(\mathbf{k}_1 \cdot \mathbf{r} + \phi) - (\mathbf{k}_2 \cdot \mathbf{r} + \varphi)$ is called the phase difference, δ. The traditional interference term is then obtained:

$$I_{12} \propto \mathbf{a}(\mathbf{r}) \cdot \mathbf{b}(\mathbf{r}) \cos(\delta) \tag{2.11}$$

I_{12} can take negative and positive values. When the contribution is negative, it is said that the interference is destructive and it is constructive otherwise. Also, term $\mathbf{a}(\mathbf{r}) \cdot \mathbf{b}(\mathbf{r})$ gives an important condition: for interference to occur the wave must not have orthogonal polarization states. Another condition for interference is that the light is coherent enough.

Let us consider the simplest case when the two waves are collinear and have the same polarization state, then, the dot product, $\mathbf{a}(\mathbf{r}) \cdot \mathbf{b}(\mathbf{r})$, can be expressed in relationship with the product of the absolute value of each one, by2.12:

$$\langle \mathbf{E}^2 \rangle = \frac{1}{2}|\mathbf{a}|^2 + \frac{1}{2}|\mathbf{b}|^2 + |\mathbf{a}(\mathbf{r})||\mathbf{b}(\mathbf{r})| \cos\delta \tag{2.12}$$

Then in terms of the total intensity, it gives us 2.13.

$$I = I_1 + I_2 + 2\sqrt{I_1 I_2} \cos\delta \tag{2.13}$$

As it can be seen from the previous equation, the relative intensity of each wave is vital. For example, if one is much stronger the interference effect may not be appreciated. This concept is known as fringe contrast and it is defined as the ratio of the amplitude of the waves. From 2.13, we can also find the maximum and minimum of the total intensity, that is found when δ is equal to $2n\pi$ and $(2n+1)\pi$ respectively with $n \in \mathbb{Z}$. For the particular case when the two intensities are equal, the maximum intensity is $4\,I_1$ and the minimum is 0, and it is where the maximum of contrast is obtained.

2.1.3/ HOMODYNE INTERFEROMETER

The main characteristic of the homodyne interferometer is that the waves that interfere have the same optical frequency, and Equation 2.13 works. In the case of the amplitude

splitting interferometers the waves that interfere come from the same source that is spitted. The phase, ϕ, of a wave that travels a distance s, is given by2.14 with ϕ_0 the initial phase of the wave,

$$\varphi = k\, n\, s + \varphi_0 \tag{2.14}$$

Now, if the out of plane displacements is $f(t)$, the phase difference δ is given by,

$$\delta = \phi - \varphi = \phi - 2\, k\, n\, f(t) \tag{2.15}$$

The factor 2 comes from the fact that the beam will be reflected from the sample. Now let us consider that the function $f(t)$ is in the form of a sinusoidal vibration with amplitude A, frequency ν, and phase θ. Combining the equation 2.15 and 2.11 give us 2.16.

$$I_{12} = C\cos\left(\phi - 2kA\sin\left(2\pi\nu t + \theta\right)\right) \tag{2.16}$$

With C the product of the amplitude of the waves and ϕ the phase difference. After some algebra we obtain 2.17

$$I_{12} = C\cos\left(\phi\right)\cos\left(2kA\sin\left(2\pi\nu t + \theta\right)\right) - C\sin\left(\phi\right)\sin\left(2kA\sin\left(2\pi\nu t + \theta\right)\right) \tag{2.17}$$

Is it possible to use the Jacobi–Anger expansion, 2.18 to expand the expression [13].

$$\mathrm{e}^{iz\sin(\alpha)} = J_0\left(z\right) + 2\sum_{n=1}^{\infty}\cos\left(2\,n\alpha\right)J_{2\,n}\left(z\right) + 2\,i\sum_{n=0}^{\infty}\sin\left(\left(2\,n+1\right)\alpha\right)J_{2\,n+1}\left(z\right) \tag{2.18}$$

Where J_n is the n-th Bessel function of the first kind. Where as $z = 2\,k\,A$ is a real positive number, it is possible to associate the real part of the expression with $\cos\left(\sin\left(\alpha\right)\right)$, and the imaginary part with $\sin\left(\sin\left(\alpha\right)\right)$. As result we obtain:

$$\begin{aligned} I_{12} = C\cos\left(\phi\right)\left(J_0\left(2\,kA\right) + 2\sum_{n=1}^{\infty}\cos\left(2\,n\left(2\,\pi\,\nu\,t + \theta\right)\right)J_{2\,n}\left(2\,kA\right)\right) \\ - 2\,C\sin\left(\phi\right)\sum_{n=0}^{\infty}\sin\left(\left(2\,n+1\right)\left(2\,\pi\,\nu\,t + \theta\right)\right)J_{2\,n+1}\left(2\,kA\right) \end{aligned} \tag{2.19}$$

For amplitude of vibrations $A \ll \lambda$, it is possible to make the approximations $J_0(2kA) \approx 1$,

$J_1(2kA) \approx \frac{1}{2}(2\,kA)$ and $J_n(2kA) \approx 0$ for $n > 1$. So the equation 2.19, then becomes:

$$I_{12} \approx C\cos(\phi) + 2\,kAC\sin(\phi)\sin(2\,\pi\,\nu\,t + \theta) \tag{2.20}$$

This equation is the general equation for homodyne systems.

2.1.3.1/ QUADRATIC POINT

From Equation 2.20, it can be appreciated that the amplitude of the signal will depend on ϕ. The best operating point for measurement of this vibration is when $\cos(\phi) = 0$, and $\sin(\phi) = \pm 1$, because we have a maximum and linear response. This happens for values of $(2n+1)\pi/2$, with $n \in \mathbb{Z}$. This points are called the positive or negative quadratic points, depending if it is located in a positive or negative slope of the $\sin(\phi)$. As illustrated in Figure 2.3.

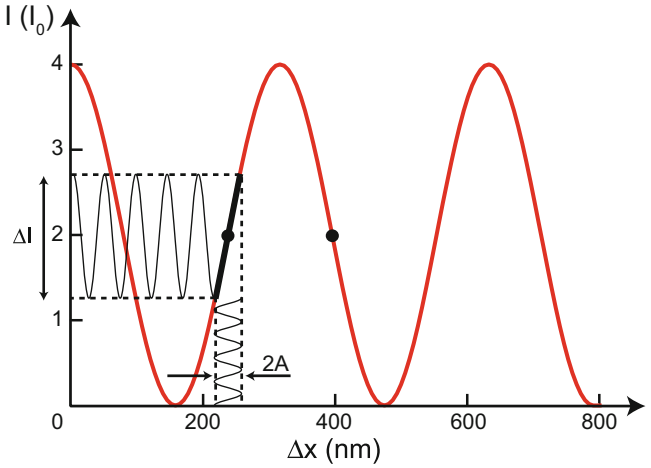

Figure 2.3: . A homodyne laser interferometer signal due to a moving object schematically presented, assuming equal optical powers and perfect interference (ideal conditions). Among the characteristics of an ideal case, the so-called quadrature-point, marked with a *black dot* is where the optimum operation point of the interferometer offering maximum sensitivity and linearity is found. The smallest object movement with an amplitude A results in a largest change in the detected light intensity *I* is shown in this operation point. [14].

There are multiple ways to work in the quadratic point depending on the type of interferometer. One of the ways is by adjusting the arm length of one of the arms. Another way is with a tunable laser and select the proper length wave to be at the quadratic point, these are more suitable in the optical fiber system based inteferometers. Then, the system is wanted to work at the quadratic point but a simple adjustment of the mirror is not enough. The phase difference ϕ will have a high dependency on ambient factors, such as drifts,

temperature changes or external vibrations. These will affect the position of the system. For that reason, a way of making sure that the interferometer is at the quadratic point is pivotal. There are mainly two forms of assuring this, one is the stabilization of the system with a feedback controller and the second is the searching of the quadratic point.

2.1.3.2/ STABILIZED HOMODYNE INTERFEROMETERS

The use of a piezoelectric controller reference mirror to make an active stabilization system was first proved by White, R. G. in 1985 [15]. But it was not used for the measurement of high frequency ultrasonic acoustic waves until 2000 by Graebner, J. E. [16]. His configuration is shown in Figure 2.4. It is a Michelson interferometer and the control of the movement of the reference mirror presented in, [16]. The reference mirror moves at 1 kHz with an amplitude of approximately $\lambda/10$, the signal detected at the photodiode D is then split and connected to two lock-in amplifiers, one tuned to 1 kHz and the other to the 2 kHz. The first is used for the calculation of the amplitude and the other one is used to provide an error signal for a feedback controller to lock the system in a Quadratic Point. This is true because the signal out at 2 kHz is proportional to the derivative of the signal. The sensitivity of the system is reported to be 0.003 Å and bandwidth limited for the detector in this case 6 Ghz.

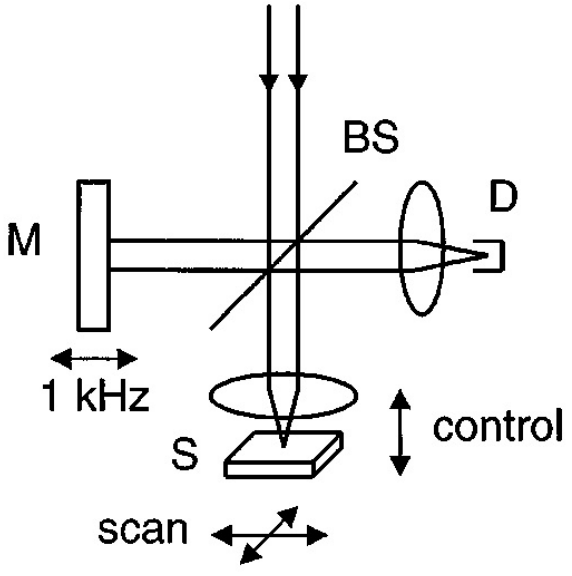

Figure 2.4: Optical setup of a homodyne Michelson interferometer with M as the reference mirror, S the sample, BS beam splitter and D a photodiode, take it from [16].

The difficulties of this method are the high cost of the equipment required to the system since at least 2 phase-lock amplifiers are needed. In this particular setup the signal of the sample is also modulated and another phase-lock amplifier was used for the demodulation. This system functions for time and frequency responses, also it has been utilized to calculate the ultra high quality factor $(5 \cdot 10^7)$ of a SiN membrane resonator at 2 MHz [17].

2.1.3.3/ QUADRATURE DETECTION HOMODYNE INTERFEROMETERS

Feedback control is not the only way to make along the measurements at the quadratic point. The other way is to move the reference mirror a couple of fringes to find the quadratic point. The working principle is the linear sweep of the reference arm a couple of wavelengths, in such a way that it is passed over several quadratic points. This method was first presented in 1969 by Sizgoric, claiming a 10^{-2}Å resolution and direct phase measurement [18]. It was again used for the scanning in 2000 by Knuuttila [19]; this method is called quadrature detection. In 2010 a Michelson based without a stabilizing system was presented by Lipiäinen et al. [20].

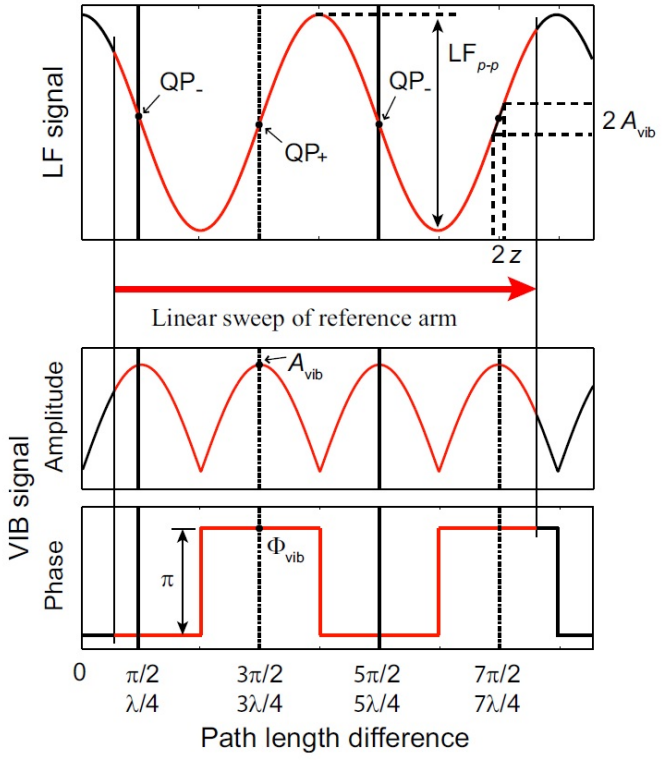

Figure 2.5: Qualitative illustration of the low frequency term top curve and the vibration term (VIB) at the bottom. [20]

.

The optical setup is the same as the one shown in Figure, 2.4. The working principles are shown in Figure 2.5. The reported sensitivity is down to 1 pm and the upper frequency is limited by the detector. The main advantage of this configuration is the simplicity and low cost of the system. As in the stabilized interferometer case, this can also work in both frequency and time domain.

2.1.4/ DIFFERENTIAL INTERFEROMETERS

Differential interferometers are based on the interference of two waves that have a time delay rather than a phase or a frequency [21].

Figure 2.6 presents the schematic of a Sagnac interferometer [22] which principal characteristic is that the optical path of both waves is the same but in opposite direction. This gives the advantage of making the setup insensitive to low frequency fluctuations, for frequencies lower than the inverse of the optical path time delay Δ_τ. The equation 2.21, shows the intensity expected from the interferometer with an vibration with the form of $A\sin(2\pi\nu t)$

$$I \propto I_0 \pm 4I_0Ak\sin(\phi_t)\cos(2\pi\nu t - \phi_t) \tag{2.21}$$

With the phase $\phi_t = \pi\nu\Delta_\tau$. From this equation it can be seen that to optimized the measurement is when $\Delta_\tau = (2\nu)^{-1}$.The time delay was set to be 0.167 ns, this gives us the capability to measure up to 3 GHz.

The bandwidth was reported to range from 10 MHz to 2.5 GHz, again with the upper frequency limited by the photodiode, and the lower frequency limited by the electronics. The net amplitude measurement response is not presented in this work. For the demonstration a BAW resonator operating a 2 GHz was used along a SAW device with resonance frequency of 936 MHz.

For the signal detection, the signal was modulated with a 10.7 MHz signal and then a lock-in amplifier was used for the measurement of the amplitude and phase. This type system can, however, be difficult to manage, the beam sizes of the two waves have to be co-linear at every point.

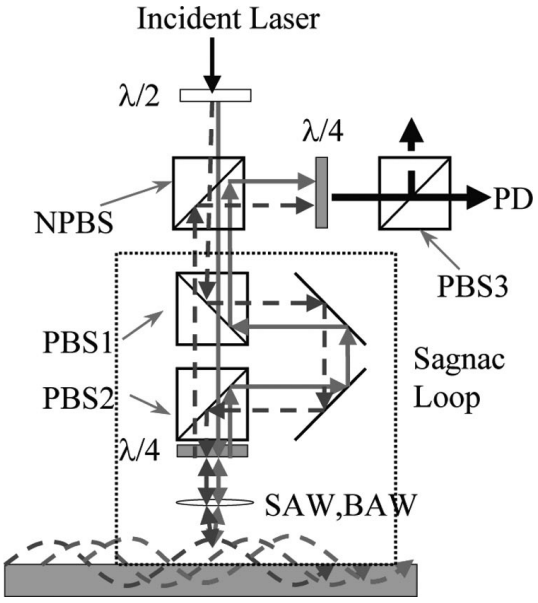

Figure 2.6: Optical configuration of a Sagnac interferometer, taken from[22]

A differential interferometer but based on a Michelson was recently adapted by Shaw A. [23]. This setup was borrowed from Monchalin et al. [21]. The schematic is shown in Figure, 2.7. Where the beam of the laser is focused to the sample.

With the help of a polarizing beam splitter and a quarter-wave plate, the beam is reflected to enter to the interferometer. Two photodiodes are utlized, one slow to conduct the feedback control and a fast one to measure the sample vibration.

The capability of this system will be strongly correlated with the path length difference. The time capability of this system will be denoted by the arm difference, for this case was optimized to a time delay of 10 ns and a frequency between 200 MHz and 400 MHz. With this measurements a detection limit of 40 pm was reported. The main advantage of this system is the simplicity of the setup and the low cost of the implementation.

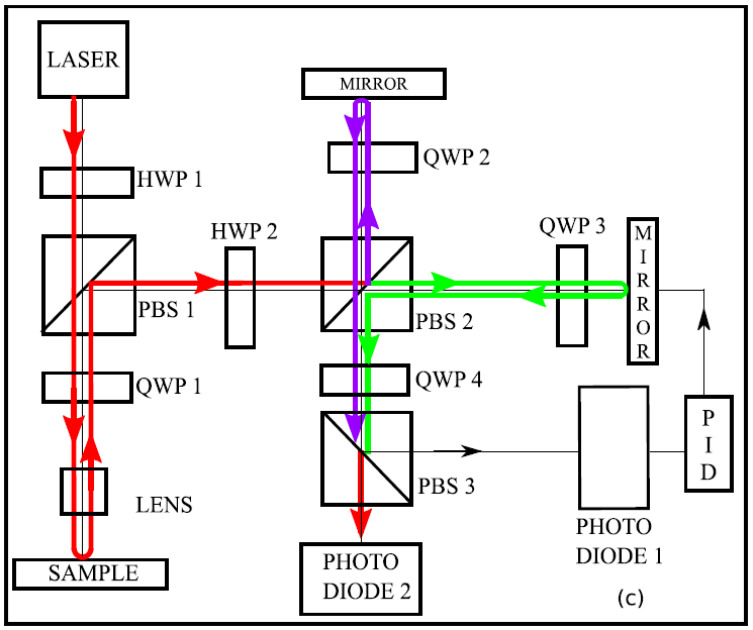

Figure 2.7: Full schematic of the differential interferometer, with active stabilization [23]

2.1.5/ Heterodyne Interferometer

A heterodyne interferometer is a kind of interferometer where the two interfered waves have different optical frequencies. The main difference with the homodyne interferometer is that the two interfering waves have a shift in frequency between them [24]. This shift is normally introduced by one or several acousto-optical modulators (AOM).

The AOM is a device where an acoustic wave is introduced to a translucid block. This wave will generate a periodic vibration of the refraction index creating a diffraction gritting. The light is diffracted in m-orders each one at a different angle. The frequency of the light, f, will be drifted as $f + mf_m$, with f_m the frequency of the acoustic wave.

The interference of this two waves provoke a modulation of the intensity, due to a beat effect, with a frequency equal to the difference of the wave frequency that normally is the order of a few tens of MHz.

One of these waves interacts with the sample and the vibration will show up as proportional to the phase of the modulated signal. The main advantage of these systems is that they are blind to a low frequency and direct retrieval of amplitude. The interference term is given by

$$I_{12} = I_1 + I_2 + 2\sqrt{I_1 I_2}\cos\left(2\pi f_m t + \phi(t)\right) \tag{2.22}$$

with f_m the frequency modulation and $\phi(t)$ as the optical phase difference.

Kokkonen et al. presented an amplitude and phase sensitive Mach-Zehnder heterodyne interferometer where an AOM is placed in the output of the beam [25]. The first order is used as a reference signal and the 0-order is used to interact with the sample. The schematic of the setup and a typical frequency response is shown in Figure, 2.8. Using the complex amplitude of the peaks found at the modulation frequency f_m and the sum with the vibration frequency f_v, it is possible to measure both the amplitude and the phase of the acoustic vibration.

This setup reported a sensitivity of $2/cdot10^{-13}m/\sqrt{Hz}$ and an upper frequency limited by the detector 6 GHz. The difficulties are to exhibit a detection limit of the signal processing and the detection of the phase response.

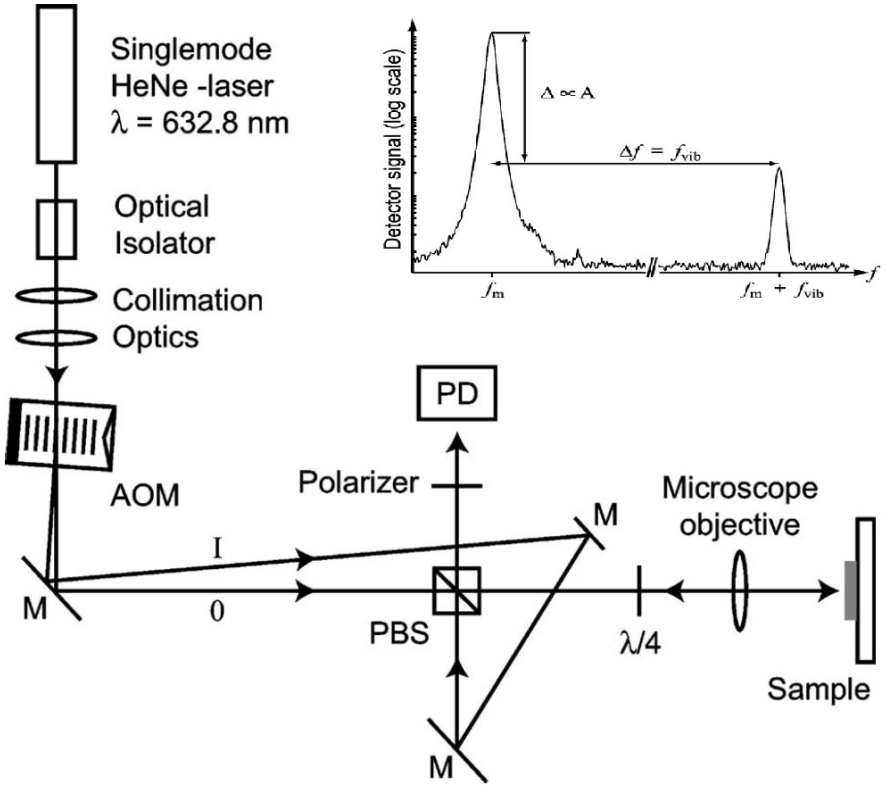

Figure 2.8: Optical setup of a heterodyne Mach-Zehnder phase and amplitude sensitive interferometer. Inset: Typical frequency spectrum of the PD, with f_m the frequency modulation and the satellite signal at shift at the frequency of the vibration f_v,. Adapted [25].

One of the limitations of the past setup is the relatively low sensitivity. Also, the amplitude and the phase can not be obtained directly, but with calculations. That is why Martinussen [26, 27] utilized a complex demodulation system, where the tuning of f_m is needed. In this arrange, the f_m has to be tuned to be close to the sample frequency. For that reason, two AOMs were used allowing a measurement range from 100 kHz to 1.3 GHz.

By focusing the beam to the AOMs, the efficiency of the optical conversion can be increased up to 70% and also will reduce the deflection of the beam. Summed to a precise control of the input frequency to the AOMs, it was succeeded to obtain $7.1 fm/\sqrt{Hz}$.

The setup shown in Figure 2.9, this is a a Mach-Zehnder interferometer with the two AOMs in the reference arm. First, the beam passes through a half-wavelength plate that will allow us to tune the power ratio between each arm. At that point, the beam is splitted into two with a polarizer beam splitter and then it is recombined by an ordinary beam splitter.

The other arm of the inferometer will focus the beam to the sample and thanks to the quarter- wavelength plate. One important thing to notice in this setup is that the high frequency is not limited only by the photodetector. As we mentioned earlier, the high frequency will depend on the capabilities of the AOMs.

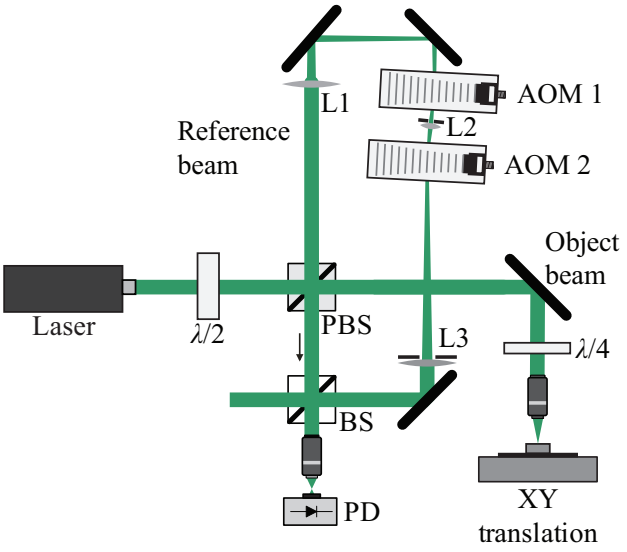

Figure 2.9: Sketch of the optical setup, taken from [27].

The main problem with this configuration is the high cost and complexity of the electronics needed such as two lock-in amplifiers, 3 low frequency generators (kHz), and 3 high frequency generators (MHz-GHz), two for the AOMs and one for the sample. An advantage

is its outstanding sensitivity and the direct measurement of the complex vibration signal.

2.2/ Detection Limit

Wagner [28] shows the steps to calculate the minimum detectable amplitude, that is generally limited by the photodiode noise. The noise of the photodiode has different sources such as the quantum noise and the thermal noise. First, we considered the current that photodetector produces, I_D that is given by,

$$I_D = P_D \frac{\eta q}{h\nu} \tag{2.23}$$

where η is the detector's quantum efficiency, h is Planck's constant, q is the carrier charge, ν the optical frequency and P_D is the optical power at the detector. For the quantum noise is

$$\left\langle I_q^2 \right\rangle = 2q\Delta\nu \left\langle I_D \right\rangle \tag{2.24}$$

with $\Delta\nu$ as the bandwidth of the detector. Now, let's calculate the signal to noise ratio ignoring the thermal noise (SNR), since its value is much lower than the quantum, it can be expressed as:

$$SNR = \left(\frac{\left\langle I_s^2 \right\rangle}{\left\langle I_q^2 \right\rangle} \right)^{1/2} \tag{2.25}$$

The I_s would be the intensity of the signal that we want to measured, for the interferometers is I_{12}, and in knife-edge is the difference of the two signals, ΔI. The limit of any measurement is reached when the signal to noise ratio is equals to 1, from there, the limit can be calculated. Following these steps, we can calculate the teorical limit of different interferometers, for example: For a wavelength of 632.8nm and a power of 1mW, and η of 10% we have a theoretical minimum detectable displacement of $5.56\times10^{-15}m/\sqrt{Hz}$ for the Michelson homodyne, $7.94\times10^{-15}m/\sqrt{Hz}$ for the Michelson heterodyne, $14.6\times10^{-15}m/\sqrt{Hz}$ for the Sagnac, interferometers and $8.03\times10^{-15}m/\sqrt{Hz}$ for the knife-edge. This values are just to have an idea of the theoretical values of the most common setups.

2.3/ DISCUSSION

Optical based vibrometers are a pivotal part for the measurement of vibration of surfaces, and there are a lot of different options. For the correct selection of the method it is important to understand what are the main advantages and disadvantages of each system, as well as the specific necessities and possibilities.

First, the light sources have to be selected according to their characteristics such as wavelength, power, coherence; then a technique has to be chosen. The knife-edge approach is the simplest if you want to stay in the tens of nanometer range, one important issue is the speckles that can lead a decrease of the SNR. In interferometeric techniques, it is important to take into account all the advantages and disadvantages as well as the desired frequencies and amplitude that you want to measure.

For homodyne interferometry, the main issue is the sensibility to the external noise. For the differential interferometric techniques the most important is phenomena duration time, for relatively long time phenomena the arms difference can be difficult to implement for example 10m for 33 μs. In heterodyne systems the signal is modulated so the issues are the demodulation of the signal and the direct measurements of the phase, which may lead to use expensive equipment. In any case the upper detection limit is determined by the conjunction of the optical detector and the electronics used. For this research thesis, a Michelson interferometer was chosen because of its versatility and wide frequency response range, also because of the possibility of characterization temporal dynamics.

3

STABILIZED MICHELSON INTERFEROMETER

As it was described in the previous chapter, a Michelson Interferometer was selected for multiple reasons, specially its versatility, simplicity and relative low cost. To overcome the low frequency fluctuation problem, two systems were implemented: an active feedback control and a quadratic point location function. The setup is shown and described below.

3.1/ WORKING PRINCIPLE

The Michelson interferometer was first introduced by Albert Abraham Michelson in 1887 [29]. Figure 3.1 shows a simplified version of the setup.

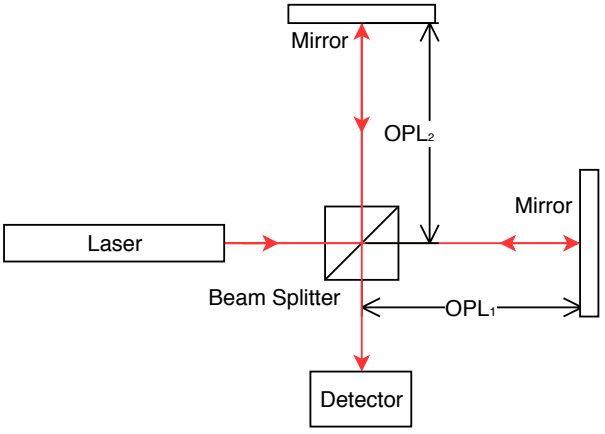

Figure 3.1: Schematic of a basic Michelson interferometer, OPL (optical path length).

Where OPL_1 and OPL_2 refer to the optical path lengths, which are simply given by the distance of the arm s multiplied by the index of refraction of the medium, for arms 1 and 2, respectively. The phase difference, δ, can be calculated from equation, 2.13,

$$\delta = 2kn_a(\Delta s) \tag{3.1}$$

The total intensity is then

$$I_{12} = 2\sqrt{I_1 I_2}\cos(2kn_a\Delta s) \tag{3.2}$$

As the wave vector k is constant, we have a minimum at $I_{12} = -2\sqrt{I_1 I_2}$, when $2kn_a(\Delta s) = (2n+1)\pi$, and a maximum $I_{12} = 2\sqrt{I_1 I_2}$, when $2kn_a(\Delta s) = 2n\pi$, with $n \in \mathbb{Z}$. Hence, when the distance difference are $(\Delta s) = \lambda(2n+1)/4$ we have constructive interference and $(\Delta s) = \lambda n/2$ we have destructive interference. Therefore, the distance between a minimum and maximum is a multiple of $\lambda/4$.

One of the mirror will be the sample with small vibration $A \ll \lambda$, using Equations2.20 and 3.3.

$$I = I_1 + I_2 + C\left(\cos(2kn_a\Delta s) + 2\,k\,A\,C\sin(2kn_a\Delta s)\sin(2\,\pi\,\nu\,t + \theta)\right) \tag{3.3}$$

Assuming that we measure is made at a quadratic point, the equation of total intensity is then given by

$$I = I_1 + I_2 \pm 2\,k\,A\,C\sin(4\,\pi\,\nu\,t + \theta) \tag{3.4}$$

With a sign depending on where the quadratic point is positive or negative. If we consider only the amplitude, A can be calculated as follows with V_s the peak amplitude of the voltage signal from the photodetector.

$$A = \frac{V_s}{2kC} \tag{3.5}$$

Finally in terms of the wavelength λ.

$$A = \frac{\lambda V_s}{4\pi C} \tag{3.6}$$

C is the maximum amplitude possible of the interference signal I_{1_2}. For the same polarization state we have the following equation, 3.7.

$$C = 2\sqrt{I_1 I_2} \tag{3.7}$$

This value can be measured by moving one of the mirrors a whole cycle. But, it also can be calculated from a good calibration and monitoring the non interference term $I_1 + I_2$. It is also calculated by the modulation of the interference signal with the vibration of the reference mirror at fix frequency. The amplitude of the modulated signal will be proportional to C. The main disadvantage of this method is the demodulation that can be complicated or expensive.

3.1.1/ NOISE LIMIT

As mentioned in the previous chapter, the noise limit can be calculated theoretically. Below, we can see the case of a Michelson interferometer.

If we define Γ as the contrast between the amplitude of the electrical amplitude, using equation 2.25 and 2.20 as I_s and 3.3 as I_D. We reach at the SNR calculation, equation bellow 3.8, we just have to remember that $\langle \sin(\omega t) \rangle = 0$ and $\left\langle \sin^2(\omega t) \right\rangle = 1/2$, for a time long enough .

$$SNR = \left(\frac{P_0 \eta}{2h\nu\Delta\nu} \frac{(2kA\Gamma \sin(\phi))^2}{1 + \Gamma^2 + 2\Gamma\cos(\phi)} \right)^{1/2} \tag{3.8}$$

The limit of any measurement is found when the noise is equal to signal, $SNR = 1$. The minimum displacement measurement, $A_{\min}$, can then be calculated with 3.9.

$$A_{\min} = \left(\frac{2\,h\,\nu\,\Delta\nu}{P_0 \eta} \right)^{1/2} \left(\frac{\left(1 + \Gamma^2 + 2\Gamma\cos(\phi)\right)^{1/2}}{2\Gamma k \sin(\phi)} \right) \tag{3.9}$$

The noise limit will depend on the operating point as well as the power of the laser and it is possible to set the Γ accordingly as well as the lenght wave.

3.2/ SETUP DESCRIPTION

The setup that is shown in Figure3.2, consists in a linearly polarized diode laser of with a wavelength λ of 633 nm and a power of 20 mW. The beam passes through an isolator for laser stability and through a half-wave plate to control the initial linear polarization state.

It is then split into two orthogonal polarized states with a polarizing beam splitter. One part is reflected and other is transmitted. The beam reflected is set to be reference arm. While the transmitted one is the sample arm. The reference arm reflects in a mirror, and the beam from the sample arm is focused with a microscope objective to the sample.

Then, the beam from the sample reflects back where most of the light is reflected towards the ordinary beam splitter, this is possible because of the double pass of a quarter-wave plate. The beam of the reference arm reflects back from a mirror to the cube, where the beam also double pass a quarter-wave plate. At the end, the two beams are recombined with the polarizing cube splitter.

Then with an ordinary beam splitter that reflects 90% and transmits 10% (90:10) a part is reflected and the beam is split again in two, one of those parts arrives to the photodetector pd_2 (ET-2020). The other part, passes through a polarizer rotated $\pi/4$ and arrives to the photodiode pd_1 (EOT-2030).

After the polarized beam splitter, the two waves have orthogonal polarization, thus there is no interference. In other words, this photodetector pd_2 will only see the addition of the two wave intensities. For the pd_1 the waves are in a same polarization state thanks to the polarizer, so there is interference.

The mirror of the reference arm is mounted on a piezoelectric-actuated mount. This mount has three piezoelectric actuators. When all the actuators move equally, the z-axis is controlled. This piezoelectric is controlled by a DAQ from National Instrument (USB-6221).

The pd_1 is a silicon based photodetector from EOT with a bandwidth of 1.2 GHz (ET-2030). The output signal from pd_1 is split in to two using a T connector, one end connected to the high frequency signal reader, e.g. an Osciloscope or a vector network analyzer; the other end is connected to a Data Acquisition Card, DAQ, from National Instruments which is connected to the computer and is controlled using LabView.

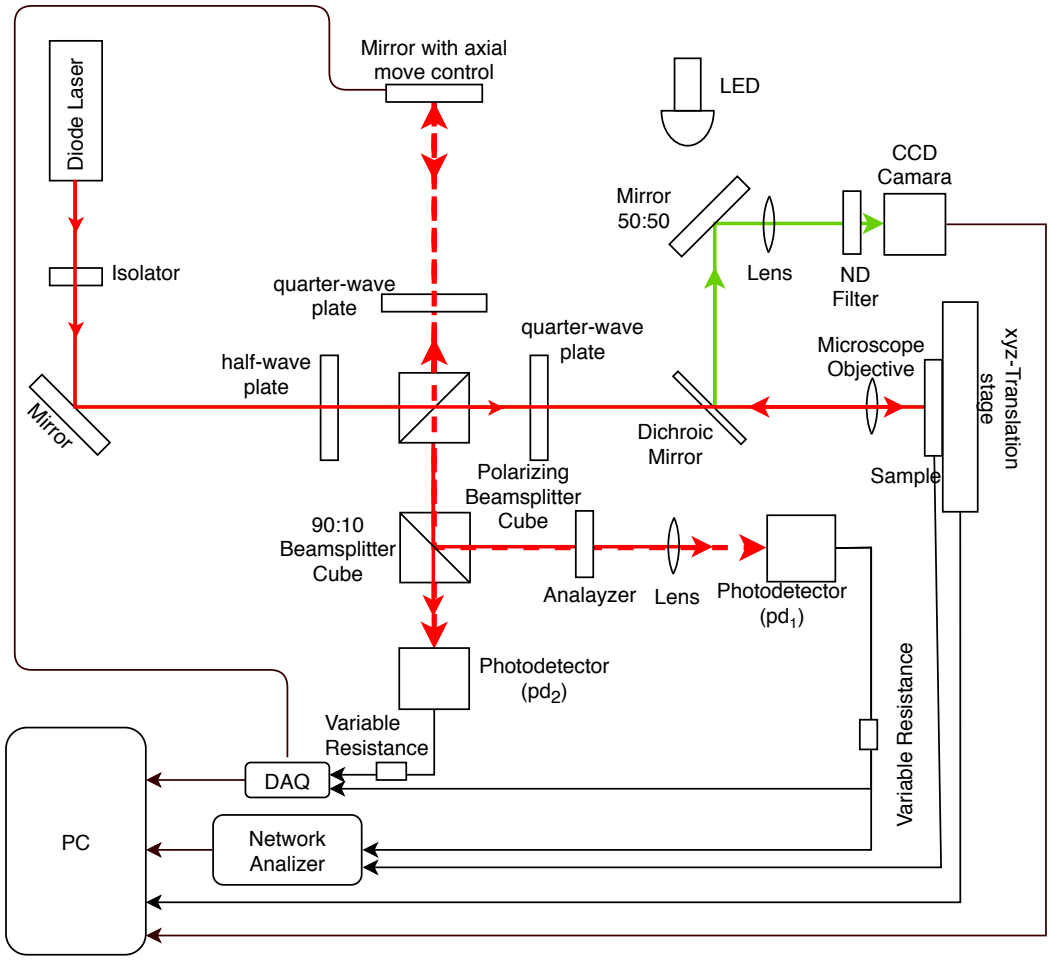

Figure 3.2: Scheme of the experimental arrangement of the Michelson stabilized interferometer. The dash line corresponds to the reference arm that uses a mirror with axial move control. The red solid line corresponds to the sample arm that is mounted on a translation stage. The image system is shown with a green line that is made with the CCD Camera and the sample is illuminated with a LED. The signals of the photodetectors are connected wit a DAQ and a network analyzer, both are controlled with a PC.

The second photodetector pd_2, is a silicon based photodetector from EOT with a bandwidth of 200 MHz (ET-2020). It is connected directly to the DAQ.

It is important to see what we aim to and in which part of the sample we are, so a imaging system is needed. For that reason, a dichroic mirror was positioned between the quarter wave plate and the microscope objective. The image is formed with the help of the 50:50 splitter and a lens is to its focal distance of a CCD sensor (DCU223C). The neutral filter (30 dB) between the CCD sensor and the lens allows to have a good general contrast of the beam that is reflected from the dichroic mirror.

A dichroic mirror helps us to selectively pass the laser beam and reflect the other colors. In the illumination system a white LED with a condenser was used. With the help of a dichroic mirror, the light goes directly to the microscope objective and then to the sample.

We can then use the Equation3.9, to calculated that the theoretical limit of this setup is $1.785 \times 10^{-15} m/\sqrt{Hz}$. Using the half-wave plate can be rotated to have a contrast Γ close to 1 and making the measurement at a quadratic point.

3.3/ IMPLEMENTATION OF THE SYSTEM

In the previous chapter, we talked about the setting of the interferometer in the quadratic point. In this section, we will talk about the implementation of the two methods to overcome these issues: the first one, and most utilized, is the stabilization of the system through a feed back controller, while the second, is the quadratic detection technique.

Let us start with the characterization of the displacement of the reference mirror by applying a triangular signal with a frequency of 1Hz and an amplitude of 10V by the DAQ, while the output signal of the pd_1 was measured with the DAQ as well. The results are shown in Figure, 3.3.

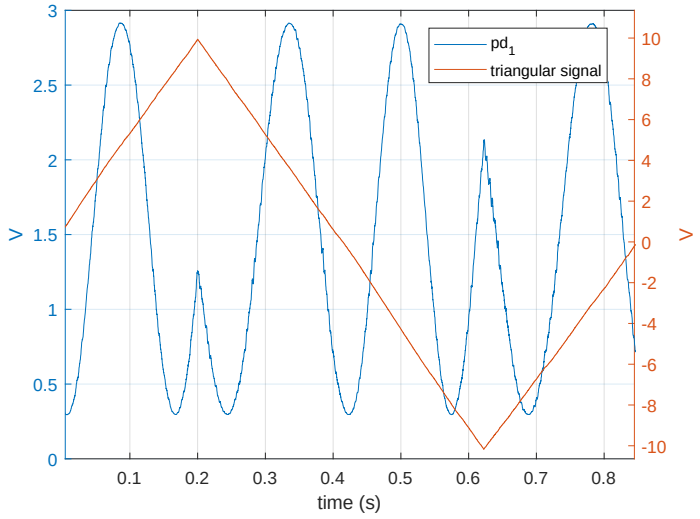

Figure 3.3: Displacement of the reference mirror by the input of one period of a triangular signal with a frequency 1Hz and a amplitude of 10V to the reference mirror by the DAQ, the output signal of the pd_1 was measured with the DAQ as well.

In t = 0.2 s and around the t = 0.6 s, we can see some peaks that represent a change of direction of the reference mirror due to the slope of the input signal swifts. These peaks, can produce an error if we want to see a repeated signal from an oscilloscope. These irregularities in the signal makes challenging to see a well-behaved signal on an oscilloscope.

Talking about the middle part between t = 0.2 and t = 0.6, where there is a constant slope of the input signal, three valleys can be seen as well as two peaks.

According to section 1, the distance between a peak and a valley for this kind of interferometer is a $\lambda/4$, for this reason during this section there were at least $5\lambda/4$. This means a displacement of at least 791 nm with a wavelength of 632.8 nm. This fits with the expects from the mount that is a maximum displacement of $\pm 4\,\mu m$ for a signal amplitude of 150 V.

Since we passed through several quadratic points, this displacement is more than enough for both methods. This signal is used for the correct calibration of the feedback control.

3.3.1/ ACTIVE FEEDBACK CONTROL

The Proportional Integral Derivative Controller (PID) was selected for the active feedback control mainly because of its simplicity, and also more sophisticated and faster controllers are not necessary because of the desired frequency and the device noise are very different. The frequency of the noise that we want to control is in a couple of Hz while the measurements are in at the MHz or even more, this means that they are very far from each other.

In Figure 3.4, a basic PID system is shown. K_P, K_I and K_D are the proportional gains for the proportional, integral and differential segments for the PID and s is the variable in the Laplace space. Here pd_2 is used as reference signal, and pd_1 is used as the feedback sensor. The signals from pd_1 and pd_2 are amplified, and each has a proportional gain K_2 and K_1, respectively.

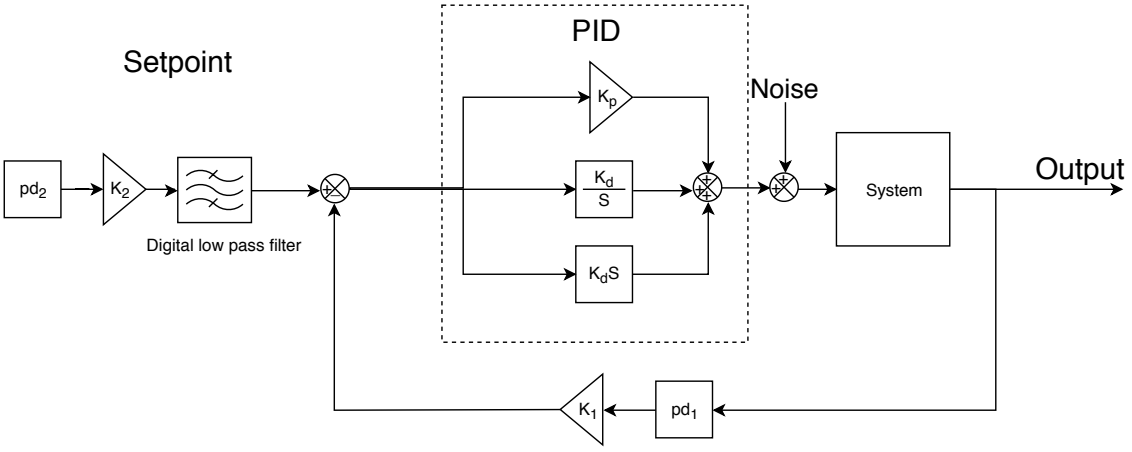

Figure 3.4: Block diagram of the active feedback control implemented.

3.3.1.1/ SETPOINT

There are two ways of measuring the quadratic point: one is by sweeping the reference mirror as in the quadratic point localization and the other one is by direct measurement. The setpoint must be at a quadratic point, and it will depend on the reflectivity of the sample since the intensity of the sample arm I_2 depends on it.

The quadratic point is when the total intensity is as shown in the Equation 3.4. At a quadratic point, the interference signal related to the vibration is going to be high frequency and low amplitude. We can approximate that the quadratic point is at $I_1 + I_2$.

For this reason it was put the pd_2 without the analyzer so there will be no interference term. The intensity seen by the photodetector is only the sum of each arm, and with that we get our reference signal. That is always related to the quadratic point. The problem is that the value of the maximum possible amplitude of the interference signal has to be calculated, but it is possible to calculate with a correct calibration of the system.

Even though the pd_2 should not have any interference term, the optics are not perfect and the interference term or a part of it may be found. That is why we want to prove if it is possible to read only the quadratic point from pd_2. That is to utilize the pd_2 as a reference signal, so any parasite signal is small enough to be ignored.

For that, we needed to find the relation between the pd_2 signal and the position of quadratic point. As mentioned earlier, the position of the quadratic point will depend on the reflectance of the measurement point. For that reason, a fixed mirror was used as the sample, and a continuously variable neutral density filter was used to simulate the change in reflectivity of the sample. The position of the filter was moved manually in order to fluctuate the light intensity.

A 100 Hz triangular signal with a 10 V amplitude was applied to the reference mirror. This will give us a signal like in Figure 3.3. From which the quadratic point can be easily obtained by measuring the offset level of the output signal. That is recorded from the pd_1 with the help of the DAQ. The signal without interference from pd_2 is also recorded by the DAQ. The result is shown in Figure 3.5. We can see that the relation is linear between the quadratic point and the pd_2, therefore we can use it as a reference signal by adding a gain with a value equal to the slope utilizing the function of the linear regression shown in Figure 3.5. This slope is the only relationship between pd_1 and pd_2.

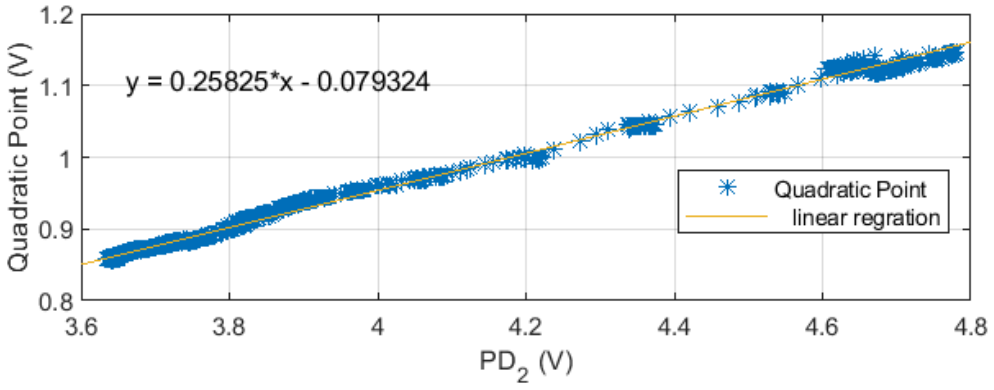

Figure 3.5: Relationship between the pd_2 and the quadratic point.

For any measurement, it is necessary to first adjust the angle of the half way plate for maximizing the visibility of the interference, we have to measure the intensity of the reference arm in terms of the pd_2, this is going to be a constant number along the measurements and a scanning. With the measurement of the intensity of the reference arm, we can get the C value, by 3.7.

With this configuration, it is possible to monitor the reflectivity. Also it is possible to use this photodiode to read in-plane vibrations using the knife-edge technique. At the same time, we can see if there are out-plane vibrations.

The change in reflectivity is not the only way to have a change in I_{12}, another source of change could be a polarization state alteration from the sample, that could happen i.e. by diffuse reflection, or a change in the wave-front, this case is more probably caused by focus error with the microscope objective. For these reasons, it is preferable to utilize an initialization process for each point than calculating the C value.

Another way to get the quadratic point in terms of the intensity is to perform an initialization process. The initialization process consists in displacing the reference mirror a couple of periods, at least one λ. With this, we will measure the C value by measuring the amplitude of the signal. Also, we will localize the quadratic point by measuring the output of the signal.

The initialization process can be as fast as the mount allows, in this case no more than 1 kHz. The main problem is that one would need to perform this initialization process for each point during a scanning. This will add time, from hundreds of milliseconds to seconds for each point, increasing the time of the total scanning.

For this setup, both of the ways were implemented with the intention to see which one was better in terms of precision and speed; nevertheless, the comparison could not be fulfilled during the period of this research.

3.3.1.2/ PID

One of the actions made to have a better noise control was to place the interferometer in an optical enclosure. Hence, an optical enclosure was used achieving a significant reduction in noise, by isolating the hole interferometer. Although, the noise level is lower than the case with no enclosure a low frequency noise is still present, this is shown in Figure, 3.6. The use of the enclosure helped to the PID implementation because the noise was diminished notoriously.

The implementation of the controller was made with LabView. The tuning of the gain values were made with trial and error approach. This is not ideal, but this is a system with high disturbance, non-linear and with random response, due to the phase difference noise. Because the response is sometimes a positive gain and sometimes a negative gain, these depend exclusively of the noise and the disturbance. For that reason, the classical step-response characterization with the black box system cannot be utilized. That is why, the trial and error approach was used with good results as seen in Figure 3.7.

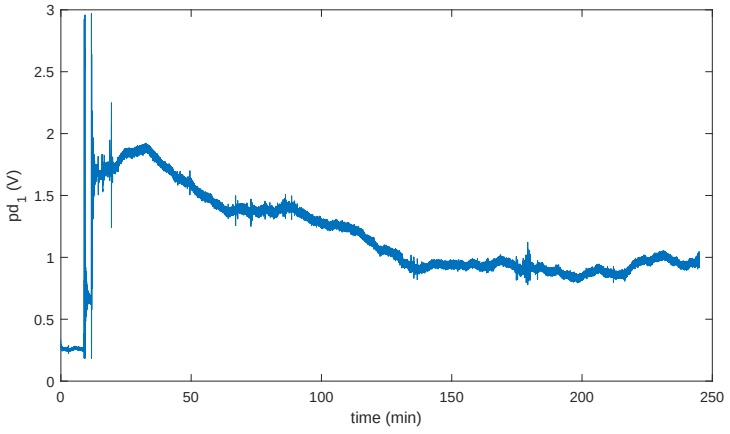

Figure 3.6: Signal from the pd_1 for ambient noise measurement.

In Figure 3.6, we can see a 20 minute noise measurement, the first two big signals are the touchings of the optical table and the following is someone closing the door of the

laboratory. We can see the noise that we want to control.

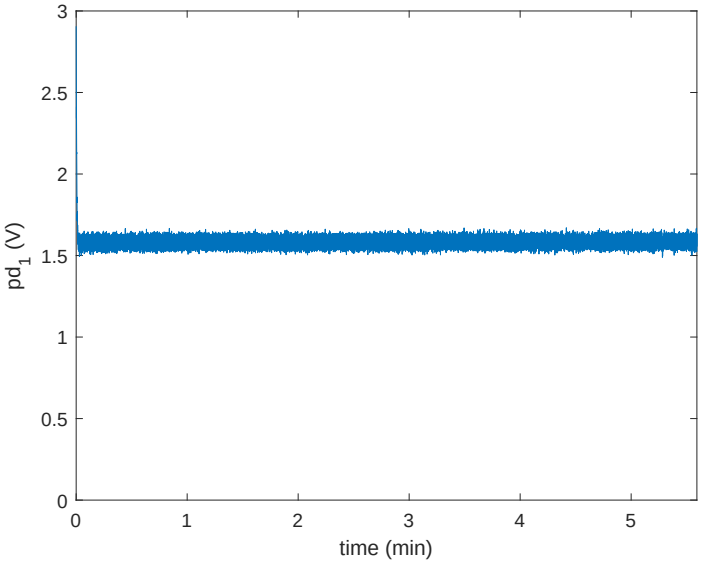

Figure 3.7: signal form pd_1 using the PID system for their stabilization.

In Figure 3.7, the stability of the system with the PID on is shown. We can say that we have a control within the margin error of an equivalent of 0.4 nm. This error should not be seen as the noise floor for the signal since this is just for the PID stability at its working frequency.

3.3.2/ QUADRATIC POINT LOCALIZATION

As it was explained in Chapter 2, the other approach to make sure that we are measuring at a quadratic point, is to perform quadratic point localization. This method consists in swifting the position of the reference mirror to achieve a couple of cycles.

This means that you have a mixing of signals, one in the high frequency, this is the one that comes from the sample, and the other of low frequency in the swifting range signal. When the signal passes a quadratic point, it triggers the measurement .

To generate the low frequency signal with an amplitude of 10 V it was used the DAQ. The frequency will depend on the required measurement time, this signal will drive the reference mirror and will move it as shown in Figure 3.3 . The signal of interference from pd_1 is simultaneously read by a low frequency oscilloscope and a high frequency oscilloscope for the sample frequency. See Figure, 3.8.

The high frequency measurement could also be done by a network analyzer, still there are more possibilities for analyzing or just capturing the signal from the sample. The detection of a quadratic point was made automatically by the oscilloscope when we couple the signal as AC and detect the positive slope at a ground level. A positive slope is used to have a positive quadratic point and a negative slope for a negative quadratic point.

To make sure that the quadratic point is always the same, the hold-off option for the trigger was used. This hold-off makes the trigger on hold until a certain time passes, this period is going to be the driven signal for the reference mirror.

Then, when the trigger is made, the trigger signal output of the oscilloscope is connected to the other equipment, this will synchronize the high and low frequencies. In such a way, we will make sure that the high frequency measurement was done in the quadratic point.

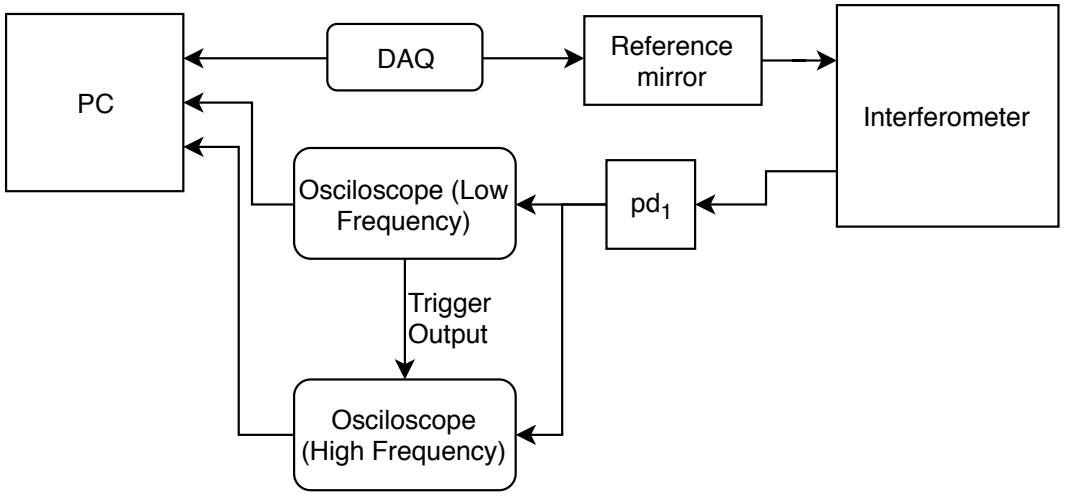

Figure 3.8: Diagram for the reading signal system uses for the non active stabilization system

With the Equation 3.10 , we can calculate the maximum time of measurement. Where ε_A is the relative acceptable error of the amplitude of the calculated displacement and f_{fl} the low frequency signal. As an example, let us consider an error of 1% for the measurement of the amplitude A acceptable, and a value of 100 Hz for f_{fl}. We have a time of $100\mu s$. To make this time larger there are two possibilities: to reduce the low frequency or increase the acceptable error. The low frequency has to be bigger than the noise to make it less sensitive to it.

$$\Delta T = \frac{\varepsilon_A}{2 f_{lf}} \tag{3.10}$$

The great advantage for this implementation is that we do not need any complicated feedback control. In this case, the DAQ was used for its simplicity and accessibility. Also, a frequency generator can be utilized to generate a low frequency signal. And there is no need of a computer if we want to make a single point measurement. This means that no complicated programming is needed. Another advantage is that we are constantly making the measurements of C each time that the quadratic point is detected. This implementation is the most robust.

On the other hand, the disadvantages of this implementation is the error that we are introducing and the limited time to measure.

3.4/ DISCUSSION

One of the issues found in the feedback controller is that if the reflectivity changes in the sample, the quadratic point can be found directly with the signal of pd_2, but the value C for the calculation of the amplitude changes as well, and it has to be calculated when it is preferable to measure it.

There was a problem of cross-talk between the DAQ and the high frequency equipment, for example an oscilloscope. A power splitter will reduce the signal. This cross-talk is presented in the moment when the DAQ makes one measurement. The cross-talk is seen as the signal shown in the following Figure3.9.

To solve the cross-talking problem, it was desired that the interval between DAQ measurements were the longest possible, but keeping a fast enough response, that is why the selected interval time was of 5 ms. This time was selected because 5 ms is also the time that the computer takes to make the PID calculations, a shorter reading time would not make any improvement. That is a possible solution, nevertheless this parasite signal remains in the measurements.

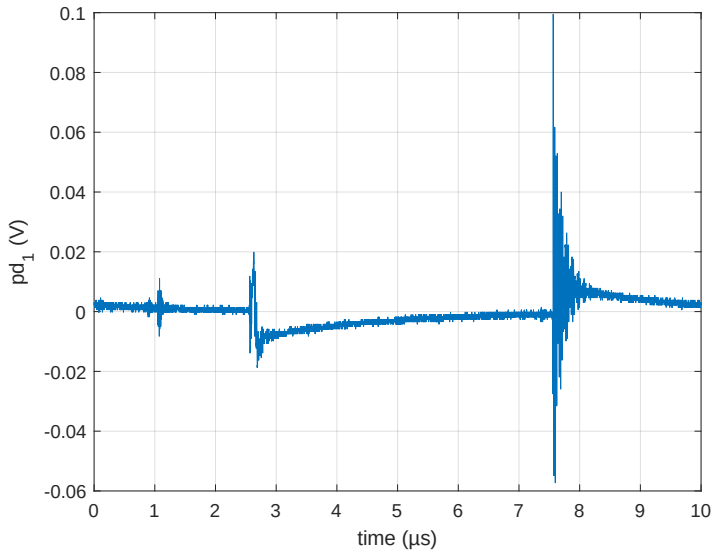

Figure 3.9: Cross talk between the DAQ and the Oscilloscope, for each measurements made by the DAQ.

There are several solutions to avoid the cross-talking, one is the use of the pd_2 as the exclusively low frequency detector, and to use it for the feedback control. With this implementation, the analyzer from the setup should be placed before the 90:10 splitter. In this case, the pd_2 would be utilized as the feedback signal and the reference signal would be a constant determined from the initialization process.

Another solution is the use of a bias tees to split the signal into two: a low frequency (lower than 10 kHz) and the high frequency that is going to be limited by the bias tees (normally more than 1 MHz). The advantage of this solution would be the inclusion of an analog low pass filter, this is needed for the feedback controller since it is always preferable to have real time response of the low pass filter. A digital filter does not give us that advantage.

For the quadratic point localization. Since we have limited time to measure, it is preferable to make the measurements with a VNA or a Spectral analyzer, both work in a the frequency domain. The bandwidth will be limited by the available time to make the measurement. If we retake the sample that we were considering above (of having an available time of $100\mu s$), this means a bandwidth of 10 kHz. Nevertheless, we have the advantages named in the Quadratic Point Localization section. Although, it is preferred to use the frequency domain, but the time domain also works.

To sum up, since no method is perfect, it is good to have the feedback control method and quadratic point localization method as options, depending of the kind of measurements

desired.

The performance expected from this interferometer is then a detection limit of $1.785 \times 10^{-15} m/\sqrt{Hz}$ and a frequency limit by the high speed detector of 1.2 GHz. A response of low frequency limited by the response of the feedback control or the bandwidth of the quadratic localization is also expected. A low pass filter of 100 Hz was utilized for the feedback control, thus a inferior limit of at least 100 MHz is anticipated.

4

Experimental Results

As it was mentioned in Chapter 2, the aim of this Master's thesis research was to characterize MEMS devices, in our case that are usually , operating at frequencies from a few hundreds of MHz to a few GHz.

In his chapter, we will work with two devices that function in a lower and known frequency to have references and confirm the functioning of the setup, one of them is the mirror Mount Piezo-actuated and the other is a PZT slab, it was used a MEMS analyser from the company Polytech to measure the frequency response.

The PZT slab was selected because this device works in the same frequency range as the MEMS analyzer, also because it was expected to obtain compression modes, this requires of a smaller lateral resolution unlike the SAW device. The mirror Mount Piezo-actuated devices were chosen because we had the data sheet.

Different methods were used to test the setup versatility as well as its possible limitations. Furthermore, this chapter will describe the measurement of the Quality factor through the ring-down technique.

4.1/ Piezoelectric Mirror Mount

A Piezoelectric Mirror Mount was a known device, with known frequencies and amplitudes from the datasheet provided. Also, the sample had a good and constant reflectivity in all the surface. That it why it was convenient to begin with this kind of sample.

The sample was a mirror in a piezoelectrically actuated mount from Thorlabs (KC1-PZ/M). This mount is the same type as the one on the reference mirror. The mount has three

Figure 4.1: Mirror Mounts with Piezo Adjusters, KC1-PZ/M

axes that can be adjusted manually or by using the integrated piezoelectric bricks.

There are three piezoelectric bricks, the total displacement possible reported is $\pm 4\mu m$ for a maximum amplitude of 150 V. The three axes will be actuated simultaneously to move at the optical access. The unload piezoelectric resonance frequency is 138 kHz. The mount is shown in Figure4.1.

To ensure the measurement at the quadratic point the interferometer was stabilized using the feedback controller, described in Chapter 2. Then, the frequency response was measured in phase and in amplitude. Using a frequency generator to produce a sine wave to excite the mount. This signal was monitored with an oscilloscope that measures simultaneously the signal from pd_1.

First, with the help of LabView, a sample was excited at a certain frequency. Then, the output signal of the interference and the and the input signal was read by an oscilloscope. The frequencies were shifted in a frequency steps of 1Hz from 100 Hz to 100 kHz. The dwell time was a hundred times the period of each frequency.

The amplitude of the input signal depended on the frequency because the sample was not impedance matching from the generator and the sample. The maximal amplitude peak to peak was 100 mV.

Then, the data was saved and analyzed as following: for each step of frequency the

Fourier transform was made to measure the amplitude and phase of the interference and reference signal. Later, the reference phase was subtracted with the sample to obtain the phase response. Since the amplitude of the input signal varies, the relative amplitude is presented in Figure 4.2 in nm per V.

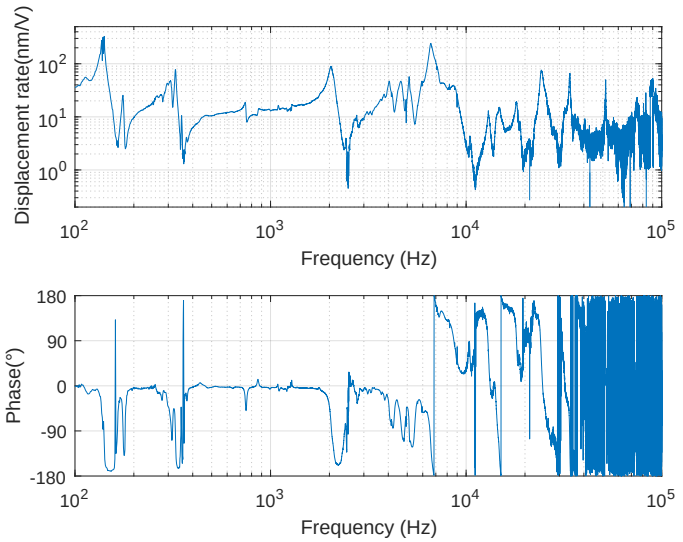

Figure 4.2: Frequency response of the mirror-mount system, from a sine signal frequency step sweeping measure with the setup.

As it can be seen, the previous figure has several modes of resonance. The first a modes near 139 Hz are believed to correspond to the mount-post system because of their low frequency.The modes at 326 Hz and at 742 Hz are the harmonics of the first resonance mode.

In Figure 4.3 is presented with the absolute amplitude of the vibration using 3.6.Where it can be appreciated that the first mode are three peaks, 137 kHz, 139 kHz and 141 kHz. Each one of the peaks correspond to each one of the piezoelectrics that are in different positions of the mount. The net amplitude response is show in Figure 4.3 where the triplet can be appreciated. The third at 2 kHz could be the main mode of the springs that are in the mount. Finally, the next mode at 6.6 kHz is believed to be the piezoelectric mode because of its relative high frequency and its phase behaviour.

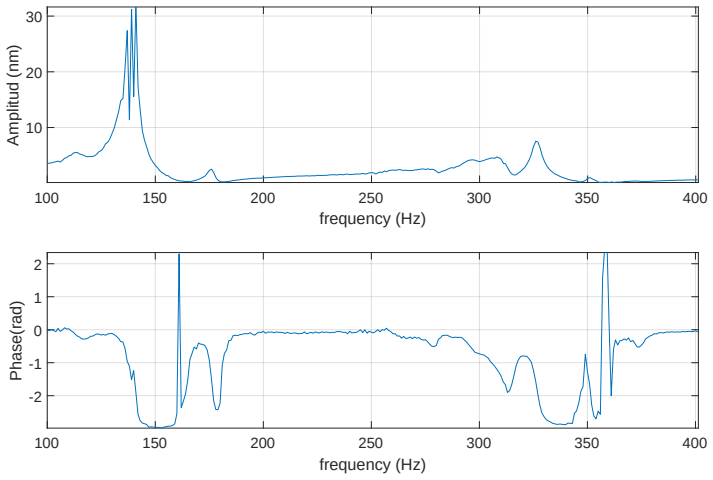

Figure 4.3: Amplitude measurement of the mirror-mount system in the range of 100-400 Hz

There is a big difference between resonance frequency found and resonance frequency of 138 kHz mentioned in the datasheet. In other words, the resonance frequency found is less than expected for some kHz. The resonance frequency was reduced because the piezoelectric had a load as was on a mount and it was pressured. also the position of the springs and screws affected in the load .

If we see the value of nm/V of the lowest frequency measure that was 100 Hz, we have a value of 3.5 nm/V. Then, we can calculate a displacement of $5.5\mu m$ for the maximum amplitude accepted for the mount of 150 V, that is close to the data-sheet value of an amplitude of $4\mu m$.

4.2/ PZT SLAB

We search to have a way to validate the setup, for that reason, we search for a device that is not too demanding. This means that it is preferable to have only compressional modes because this would allow a low lateral resolution. Also, it has to work in the frequency range of a commercially available MEMS analyzer. For that reason, a PZT slab was selected. It was expected to work in the few MHz.

The PZT was glued to a PCB and a wire was connected to the top. A square glass plate with golden patterns (for localization purposes) was glued. A wire was bond from the PZT to the PCB. The size of the PZT is about 0.5mm per side and glass of 0.3mm. The device

is shown in Figure 4.4.

Figure 4.4: The sample consist in a slab of PZT with a slab of glass glue at the top with a gold plated pattern

4.2.1/ Frequency Response

4.2.1.1/ VNA Measurements

The Vector Network Analyzer measurements will help us to characterize the S-parameters and with that the electrical response of the sample. The electrical characterization was made with a VNA, connecting to the port 1, and reading of the S_{11}parameter was made, the results are shown in Figure, 4.5 . There are several peaks left to right, 375.4 kHz, 440.8 kHz, 949.3 kHz, 1.052 MHz, 1.405 MHz, 1.805 MHz, 2.157 MHz, 2.594 MHz, 3.288 MHz, 3.806 MHz, 4.374 MHz and 4.705 MHz.

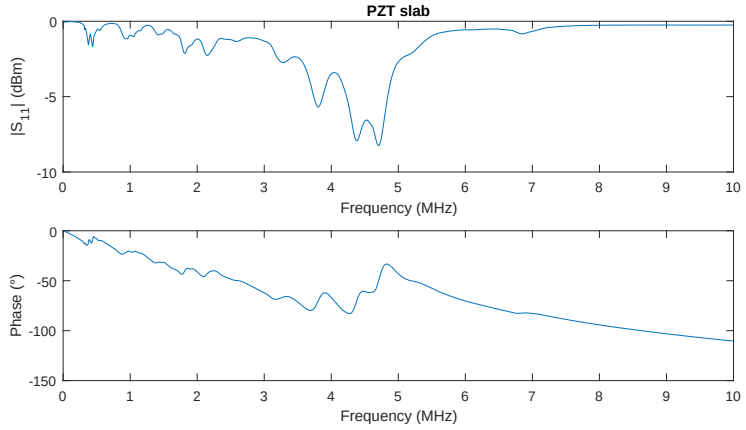

Figure 4.5: S_{11} parameter measured with the VNA of the PZT slab sample with the first two modes at 375.4kHz and 440.8kHz.

The impedance was calculated from the S_{11} parameter with the help of Matlab. The results are shown in the following Figure 4.6. The results do not give us more information than the previous graph, however it lets us to observe better the electrical behavior of the

sample. We can see in a more clear way that the modes found from 949.3 kHz to 3.806 MHz are the harmonics of the signals at 375.4 kHz and 440.8kHz, they are called radial resonances. While the signals from 4.374 MHz to 4.705 MHz are a new mode called thickness resonances.

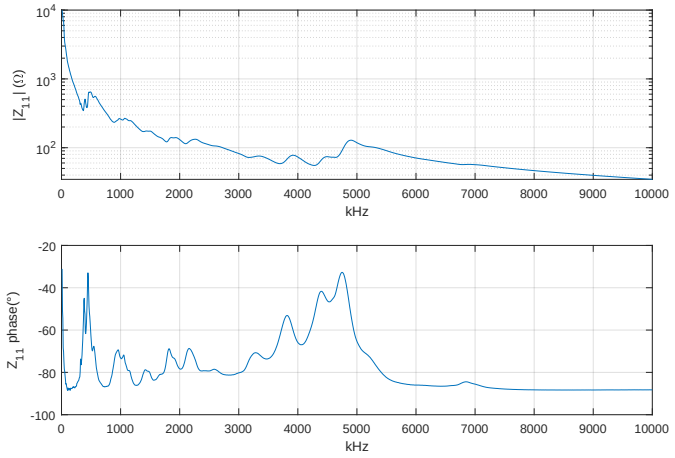

Figure 4.6: Z_{11} Impedance response of the PZT slab.

We wanted a BAW resonator. That is why it was expected that the first resonance modes were bigger, but they are not. This could be a result of the weight added to the piezoelectric.

4.2.1.2/ POLYTECH MSA-500 MICRO SYSTEM ANALYSER

This instrument is a fully integrated Structural Dynamics and Surface Metrology System. The functioning consists in focusing one beam of laser light on a spot on the sample surface in order to accurately track the position and velocity of that point.

With the vibrometer, we can measure with accuracy three main quantities: surface topography with sub-nanometer resolution; in-plane deformation and vibration modes, with nanometer amplitude resolutions and at frequencies up to 1 MHz; out-of-plane deformation and vibration modes, with picometer amplitude resolutions and at frequencies up to 24 MHz.

To achieve these functionalities, three separated non-contact measurement technologies into one piece of equipment had to be incorporated: white-light interferometry, enabling surface metrology and topography reconstruction; laser-Doppler vibrometry, enabling

real-time out-of-plane vibration analysis; and stroboscopic video microscopy, enabling real-time in-plane vibration analysis.

The vibrometer is a heterodyne interferometer type Mach-Zender, it uses an acousto-optic modulator and a laser He-Ne at 632.8 nm. This produces a frequency modulated signal, that is then demodulated by two different types of demodulators: digital and analogue. The digital measures velocities, while the analogue measures displacements. This equipment has an amplitude resolution limit of $0.1pm/\sqrt{Hz}$.

A picture is displayed in Figure4.7,[30].

Figure 4.7: Polytec MSA-500 Micro-System Analyser

A chirp signal was selected with a 10V amplitude and a frequency interval between (0.001-10) MHz. The results are shown in Figures,4.8, 4.9 and 4.10.

The first figure shows the average of amplitude and phase to understand the general behavior for the devices and other two are the field maps for the two first and strongest signals, at 375kHz and 439kHz, but it also have the signals at 901kHz, 1MHz, 1.4MHz, 1.8MHz, 2.2MHz and 3.1Mhz and 4.3MHz.

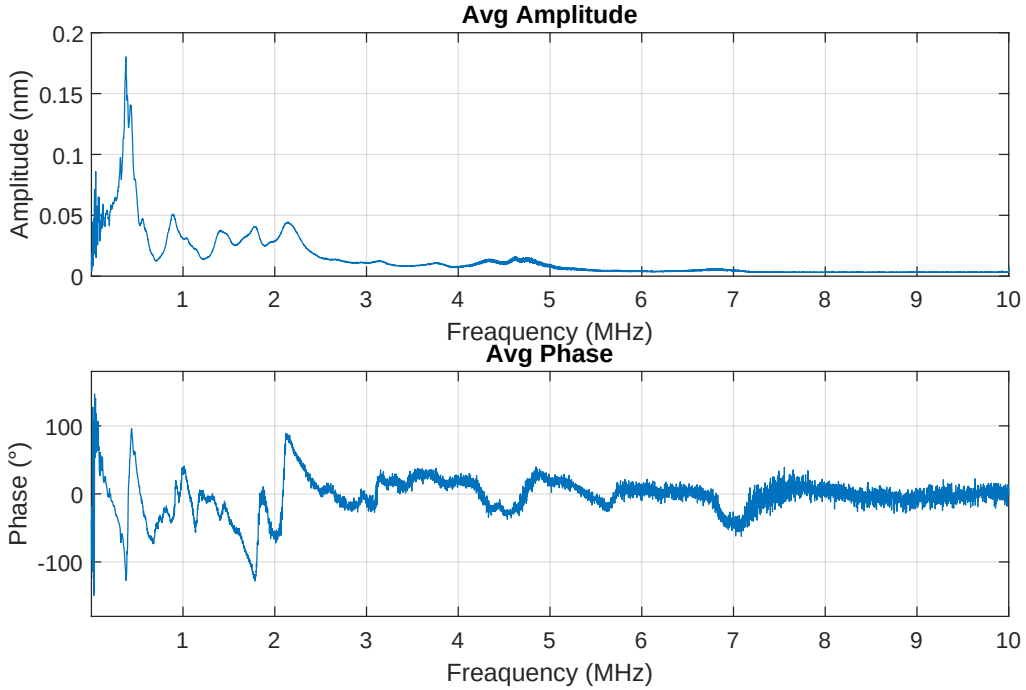

Figure 4.8: Average of the amplitude and phase from all the scanned points, with peaks at 375 kHz, 439 kHz, 901 kHz, 1 MHz, 1.4 MHz, 1.8 MHz, 2.2 MHz and 3.1 Mhz and 4.3 MHz.

The amplitude and phase field of the two main modes are presented in Figures 4.9 and 4.10.

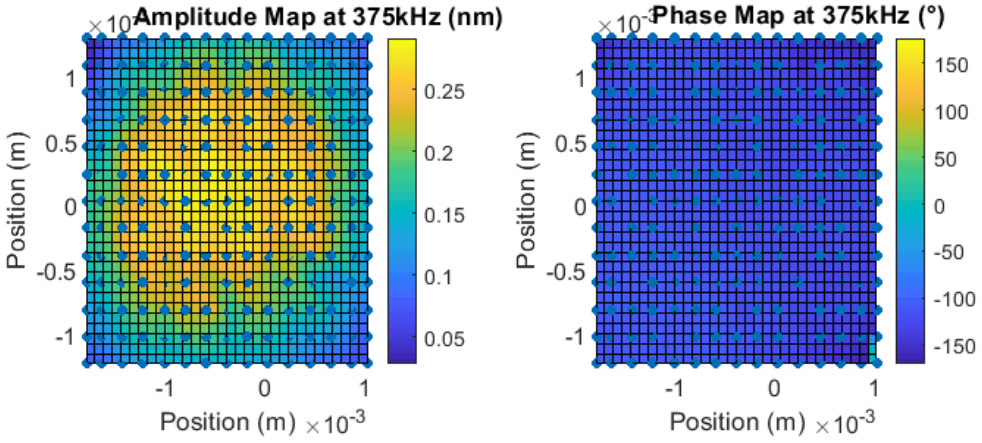

Figure 4.9: 375 khz field maps of amplitude and phase, MEMS analyzer.

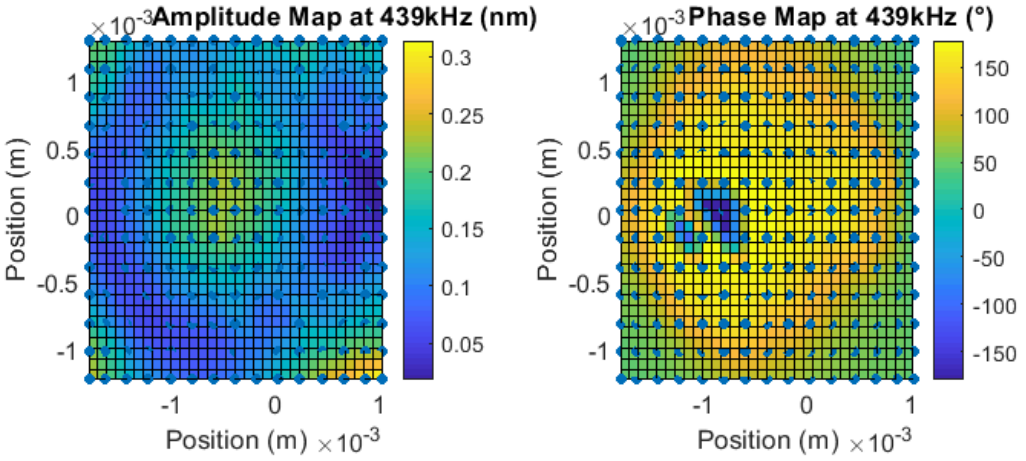

Figure 4.10: 439 khz field maps of amplitude and phase, MEMS analyzer.

At 375 kHz it was found the maximum amplitude of displacement to be 295.9 pm. Both of the modes resembles of the first vibration mode of a plate bottom fix and fully clamped of a narrow portion of the edge of the bottom. This will be the effect of the glue that spreads out. Although, the other peaks found do not resemble to any particular shape.

4.2.1.3/ SETUP RESULTS

The feedback control stabilization was selected for the characterization of the displacement with the setup. For the setup, the measurement was made in only one point (the middle of the sample) and it was used the feedback control form.

The sources signal and measurement was made with the VNA; the pd_1 was connected to Port 1 and the sample was connected to port 2, the output of the port 2 was set at +10 dBm and the port 1 output was set to -50 dBm for not to compromise the photodiode.

The sample was connected with a 50 Ω terminal, to have the correct calculation of the input amplitude voltage, 0.707 V for this configuration. The S_{21} parameter is measured after calibration of the VNA, the measurement was configured to be an average of 16 measurement with 50 Hz bandwidth.

For the net amplitude calculation Equation3.6 was used getting C from the initialization process described in the passed section and the amplitude A the multiplication of $|S_{21}|$ and the amplitude of reference 0.707 V. The results are shown in Figure 4.11.

We can see the comparison between the results of the MEMS analyzer and the setup.

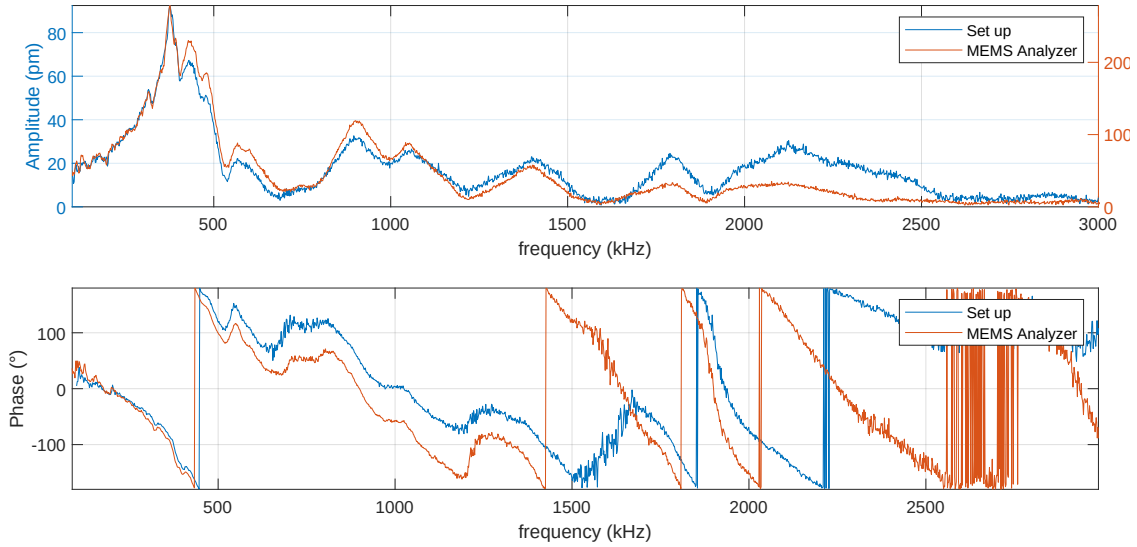

Figure 4.11: PID configuration measurement of the amplitude and phase response for an amplitude signal input of *0.707V* and the amplitude respond and phase for the same point of the sample with *10V* with the MEMS analyzer.

The main difference is the general amplitude scale from the setup to the MEMS. The MEMS analyzer have a maximum amplitude of 278 pm, while the measurements by the setup have a maximum amplitude of 92 pm, both at the first peak at 375 kHz. This is because of the difference between the amplitude of the excitation signal.

The signal of the MEMS analyzer is 14 times bigger than the one delivered by the VNA. But the difference between the amplitudes are just 3 times. This non-linearity has an unknown source.

We can see that the peaks are at the same frequency. The main difference are the modes at 1.8 MHz and 2.2 MHz where the setup presents a relatively bigger amplitude.

In this particularly measurement, the noise floor is about 2 pm. Since the bandwidth of the VNA was 50Hz, we can claim a sensitivity of at least of $0.14pm/\sqrt{Hz}$.

The concordance of the two measurements is good as can it be appreciated. For the phase, we have a general better performance of the setup. In the MEMS analyzer, the noise over 2.5 MHz was not found.

4.2.2/ Quality Factor

The quality factor is a measure of the damping of an oscillator. A high (thousands of units) quality factor is fundamental for the correct functioning of the MEMS devices, such as the

resonators, filters, sensors, among others. Besides, a high quality factor is pivotal for the tests of quantum mechanics in macroscopic systems [31].

For the measurement of the quality factor (QF) in our setup, it was used the ring-down methodology [17]. However, this is probably not the most well-suited sample because of the low amplitude vibrations and low quality factor values.

The ring-down method consists in exciting the resonator to provoke oscillation frequencies. Then, we have to observe how the amplitude of the oscillations decreases as the system returns steady. The envelope decay is normally exponential and can be modeled as given in Equation 4.1, with ω the angular frequency of the system, t the time, Q the QF and U_0 the amplitude.

$$u(t) = U_0 e^{-\frac{\omega}{2Q}t} \tag{4.1}$$

As mentioned before, we have implemented two systems, the feedback controller and quadratic detection. In this case, we utilized the quadratic detection implementation to demonstrate the capability of our system to measure a quality factor. A high speed oscilloscope (Agilent, DSO9254A) was utilized as the high frequency measurement system. The low frequency signal was suited to have the biggest bandwidth possible of 80 Hz.

A low frequency generator (Agilent, 33220A) was used to introduce a sinusoidal type signal with an amplitude of 2.5 V, the first mode of the sample was excited to 375 KHz. The length of the signal was $50\mu s$, the time can be short because the quality factor is low. With the trigger out signal from the low frequency oscilloscope, the output of the signal was synchronized exactly at the quadratic point. With this kind of signal, the resonator was excited.

The signal of the frequency generator was divided with a signal splitter, One part was utilized for the excitation of the PZT resonator while the other was connected to the oscilloscope. As it was expected, the results are in a linear trend, because of the low frequency signal and we are not utilizing anything to filter the low frequency out like a high pass filter or something more sophisticated as the use of a phase-lock amplifier. See Figure 4.12.

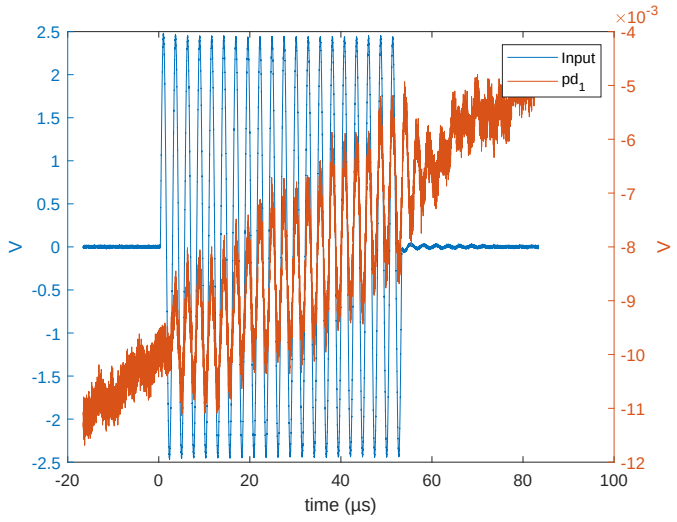

Figure 4.12: Raw signal from the high speed oscilloscope of the ring-down measurement at 375kHz, with an amplitude of 2.5 V .

To eliminate this trend, it was used Matlab by applying a high pass filter with a cut frequency of 250 kHz. This will also filter out the unwanted low frequency noise. Then, the QF value was fitted, it was found to have a value of 4 ± 2; see Figure 4.13.

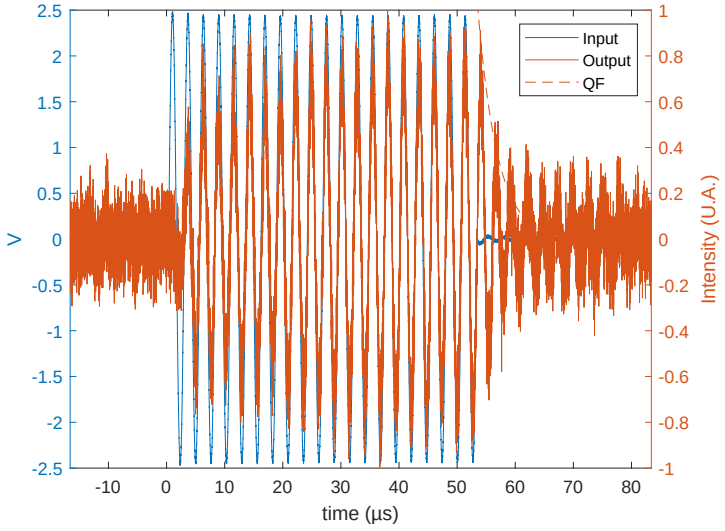

Figure 4.13: Filtered signal (red line) and with quality factor fitted (dash line) with a measured quality factor of 4 ± 2.

For the previous results, it is also possible to estimate the QF, by the formula of the frequency over the full width at half maximum, this give us a result of 2.97 for the peak at 375 kHz. Both quality factor measurements are within the margin of error of the obtained number.

It can be appreciated, as well, that there is a delay of half a period before the resonator starts to be on phase with the signal. One explanation for this delay could be, for example, that the system is a non-minimum phase (terminology from controlled theory) [32]. That means that for a step response the system has an opposite response for a short brief of time and then starts to behave normally, this can be seen as a time delay. Because there is a high level of noise, the period delay may go to the opposite way and the process could be covered by the noise.

The quality factor is low, nevertheless is inside the expected margin in concordance of the measurements from the MEMS analyzer with the setup made with the VNA and the electrical signal.

4.3/ DISCUSSION

This measurement's aim was to proof the versatility of the setup to measure at the time or frequency domain, also to have an idea of the capability of the setup. The displacement detection limit was found to be at least *4pm* for a relatively low reflectivity sample as the case of the glass.

The use of the VNA for the measurement was the simplest method because all calculations are all done by the VNA. The main issue is the limitation of 10 dBm of output signal. For a more powerful signal input to the sample, a radio frequency amplifier could be used, but this presents a risk for the VNA since the amplified reflection could be bigger than the capacity of the apparatus. Since both of the samples where lower than 10MHz a specialized amplification of the signal was not required, but if we want to use the whole capability of the photodetector, it is important to dedicate a signal amplifier.

For the quadrature detection, an issues of false trigger because of the noise, the oscilloscope could have made erroneous measurements of the quadratic point. To overcome this situation the it was used the hold-off of the oscilloscope. This forced a measurement after a certain time. This arises the time of the point to point measurement a couple of hundreds of milliseconds. This will increase the time of the measurement of the VNA for long and high precision measurements. For that reason it was used the feedback stabilization for the VNA.

5

CONCLUSION

Along this work, we have explored the implementation of a homodyne Michelson interferometer with two options of stabilization, using a feedback controller and a Quadrature detection approach.

First, we researched the state of art of the optical characterizations of the MEMS devices. The third chapter describes in detail the functioning of the apparatus and its working principals. On the other hand, the fourth chapter shows how the interferometer was used to characterized a PZT slab and a piezoelectric mount.

It was achieved to implement a homodyne interferometer for the measurement of out of plane vibration. The results of the PZT slab are comparable with the ones of the commercial setup. Our setup was proved in the frequency domain as well as the time domain.

The system was also proved to be phase sensitive and easy to measure. The resolution was found to be close to 1 pm. The frequency response from the 100 Hz to the 5 MHz was proved and is theoretically limited only by the electronics. This means a 1.2 GHz and is easily upgradeable. The amplitude limit was found to be $0.14pm/\sqrt{Hz}$, this value was found with the PZT slab with low reflectivity. So, the real value is expected to be lower. The direct measurement of the amplitude and phase was proved with the help of a VNA.

The capability of this system was not found commercially. We achieved to make the measurements in the time domain. The frequency response of a PZT slab for the out out plane displacement was measured as well as the frequency response of the mirror mount.

The measurement of the quality factor was made as well. The device proved to have a

low quality factor with a value of arround 4 by the ringdown method.

The first prospective is to make a 2D scanning, that would be horizontal and not vertical in order to have a better stability and achieve nanomentric lateral resolution, we get this by changing the translation stage and the microscope objective to have the dot at the diffraction limit. To make the sample horizontal, it is needed to elevate the interferometer and with the help of a mirror steer the beam to the sample arm.

Another improvement would be to change the diode laser for another stabilized laser, because the diode laser does not have TEM_{00} neither has a good functioning during hot weather.

Also, we have to change the division of the first photodiode from a T type for a T bias, in this way, we can divide the signal in low and high frequency signal, besides it could help us to eliminate the cross talking problem.

In addition, it is planned to change the system of the detector's amplification because the current method of variable resistor reduces the bandwidth of the photo-detectors. This method was selected because amplifiers that work in the low frequency domain were not available. This bandwidth was enough for the presented devices, but not enough for the MEMS larger than 100 MHz.

Finally, this setup will be used to contribute to the characterization of MEMS, NEMS and phononic crystals of the Phononics and Microscopy group at the MN2S department of FEMTO-ST. This will lead to a better understanding and designing of this knowledge area, this has an impact in the development of technology, specially in the area of telecommunications, sensors, vibration, isolation, among others.

BIBLIOGRAPHY

[1] R. L. Whitman and A. Korpel. Probing of Acoustic Surface Perturbations by Coherent Light. *Applied Optics*, 8(8):1567–1576, August 1969.

[2] Jean-Pierre Monchalin. Laser-Ultrasonics: From the Laboratory to Industry. *AIP Conference Proceedings*, 700(1):3–31, February 2004.

[3] Mo Li, H. X. Tang, and M. L. Roukes. Ultra-sensitive NEMS-based cantilevers for sensing, scanned probe and very high-frequency applications. *Nature Nanotechnology*, 2(2):114–120, February 2007.

[4] Olli Holmgren, Kimmo Kokkonen, Timo Veijola, Tomi Mattila, Ville Kaajakari, Aarne Oja, Jouni V. Knuuttila, and Matti Kaivola. Analysis of vibration modes in a micromechanical square-plate resonator. *Journal of Micromechanics and Microengineering*, 19(1):015028, December 2008.

[5] D. Karabacak, T. Kouh, C. C. Huang, and K. L. Ekinci. Optical knife-edge technique for nanomechanical displacement detection. *Applied Physics Letters*, 88(19):193122, May 2006.

[6] V. J. Gokhale and J. J. Gorman. Optical Knife-Edge Displacement Measurement With Sub-Picometer Resolution for RF-MEMS. *Journal of Microelectromechanical Systems*, 27(5):910–920, October 2018.

[7] H. Engan. A Phase Sensitive Laser Probe for Pulsed SAW Measurements. *IEEE Transactions on Sonics and Ultrasonics*, 29(5):281–282, September 1982.

[8] S. O. Achamfuo-Yeboah, R. A. Light, and S. D. Sharples. Optical detection of ultrasound from optically rough surfaces using a custom CMOS sensor. *Journal of Physics: Conference Series*, 581:012009, January 2015.

[9] A. Korpel, L. J. Laub, and H. C. Sievering. Measurement of acoustic surface wave propagation characteristics by reflected light. *Applied Physics Letters*, 10(10):295–297, May 1967.

[10] Giovanni Carlotti. Elastic Characterization of Transparent and Opaque Films, Multilayers and Acoustic Resonators by Surface Brillouin Scattering: A Review. *Applied Sciences*, 8(1):124, January 2018.

[11] J. R. Sanderocock. Light scattering from surface acoustic phonons in metals and semiconductors. *Solid State Communications*, 26(8):547–551, May 1978.

[12] G. Carlotti. Conventional and micro-focused Brillouin light scattering for the elastic characterization and the acoustic field mapping in SAW and BAW resonators. In *2017 IEEE International Ultrasonics Symposium (IUS)*, pages 1–1, September 2017.

[13] Milton Abramowitz and Irene A. Stegun. *Handbook of Mathematical Functions with Formulas, Graphs, and Mathematical Tables*. Dover, New York, ninth dover printing, tenth gpo printing edition, 1964.

[14] Kimmo Kokkonen. Laser interferometers in physical acoustics. In *2009 IEEE International Ultrasonics Symposium*, pages 1036–1043, Rome, Italy, September 2009. IEEE.

[15] R. G. White and D. C. Emmony. Active feedback stabilisation of a Michelson interferometer using a flexure element. *Journal of Physics E: Scientific Instruments*, 18(8):658–663, August 1985.

[16] J. E. Graebner, H. F. Safar, B. Barber, P. L. Gammel, G. J. Herbsommer, L. A. Fetter, J. Pastalan, H. A. Huggins, and R. E. Miller. Optical mapping of surface vibrations on a thin-film resonator near 2 GHz. In *2000 IEEE Ultrasonics Symposium. Proceedings. An International Symposium (Cat. No.00CH37121)*, volume 1, pages 635–638 vol.1, October 2000.

[17] S. Chakram, Y.S. Patil, L. Chang, and M. Vengalattore. Dissipation in Ultrahigh Quality Factor SiN Membrane Resonators. *Physical Review Letters*, 112(12):127201, March 2014.

[18] S. Sizgoric and A. A. Gundjian. An optical homodyne technique for measurement of amplitude and phase of subangstrom ultrasonic vibrations. *Proceedings of the IEEE*, 57(7):1313–1314, July 1969.

[19] J. V. Knuuttila, P. T. Tikka, and M. M. Salomaa. Scanning Michelson interferometer for imaging surface acoustic wave fields. *Optics Letters*, 25(9):613–615, May 2000.

[20] Lauri Lipiäinen, Kimmo Kokkonen, and Matti Kaivola. Phase sensitive absolute amplitude detection of surface vibrations using homodyne interferometry without active stabilization. *Journal of Applied Physics*, 108(11):114510, December 2010.

[21] J.-P. Monchalin. Optical detection of ultrasound. *IEEE Transactions on Ultrasonics Ferroelectrics and Frequency Control*, 33:485–499, September 1986.

[22] K. Hashimoto, K. Kashiwa, N. Wu, T. Omori, M. Yamaguchi, O. Takano, S. Meguro, and K. Akahane. A laser probe based on a sagnac interferometer with fast mechanical scan for RF surface and bulk acoustic wave devices. *IEEE Transactions on Ultrasonics, Ferroelectrics, and Frequency Control*, 58(1):187–194, January 2011.

[23] Anurupa Shaw, Damien Teyssieux, and Vincent Laude. A differential optical interferometer for measuring short pulses of surface acoustic waves. *Ultrasonics*, 80:72–77, September 2017.

[24] DANIEL ROYER and Eugene Dieulesaint. *Elastic Waves in Solids II: Generation, Acousto-optic Interaction, Applications*. Advanced Texts in Physics. Springer-Verlag, Berlin Heidelberg, 2000.

[25] Kimmo Kokkonen and Matti Kaivola. Scanning heterodyne laser interferometer for phase-sensitive absolute-amplitude measurements of surface vibrations. *Applied Physics Letters*, 92(6):063502, February 2008.

[26] Hanne Martinussen, Astrid Aksnes, and Helge E. Engan. Wide frequency range measurements of absolute phase and amplitude of vibrations in micro- and nanostructures by optical interferometry. *Optics Express*, 15(18):11370–11384, September 2007.

[27] Erlend Leirset, Helge E. Engan, and Astrid Aksnes. Heterodyne interferometer for absolute amplitude vibration measurements with femtometer sensitivity. *Optics Express*, 21(17):19900–19921, August 2013.

[28] James W. Wagner and James B. Spicer. Theoretical noise-limited sensitivity of classical interferometry. *JOSA B*, 4(8):1316–1326, August 1987.

[29] A. A. Michelson and E. W. Morley. On the relative motion of the Earth and the luminiferous ether. *American Journal of Science*, s3-34(203):333–345, November 1887.

[30] Polytec MSA-500 Micro System Analyzer (vibrometer) | IMRI.

[31] Keith C. Schwab and Michael L. Roukes. Putting Mechanics into Quantum Mechanics. *Physics Today*, 58(7):36, January 2007.

[32] Pedro Albertos and Sala Antonio. *Multivariable Control Systems: An Engineering Approach*. Advanced Textbooks in Control and Signal Processing. Springer-Verlag, London, 2004.

LIST OF FIGURES

A

JONES' MATRIX APPROACH

Using the Jones' formalize let's determinate the polarization state, we start by reminding the Jones' matrices for the rotation a certain angle θ, $\mathbf{J}_{ROT}(\theta)$, a linear vertical polarizer, $\mathbf{J}_{LHP}$, a linear horizontal polarizer $\mathbf{J}_{LVP}$, a reflecting surface with a reflectance, r, $\mathbf{J}_R$ for a mirror, $r = 1$, $\mathbf{J}_M$, and a wave plate with the fast axis in the horizontal, $\mathbf{J}_{WP}(\phi)$ with ϕ the phase difference between the fast and slow angle.

$$\mathbf{J}_{ROT}(\theta) = \begin{pmatrix} \cos(\theta) & \sin(\theta) \\ -\sin(\theta) & \cos(\theta) \end{pmatrix} \tag{A.1}$$

$$\mathbf{J}_{LHP} = \begin{pmatrix} 1 & 0 \\ 0 & 0 \end{pmatrix} \tag{A.2}$$

$$\mathbf{J}_{LVP} = \begin{pmatrix} 0 & 0 \\ 0 & 1 \end{pmatrix} \tag{A.3}$$

$$\mathbf{J}_R = \begin{pmatrix} r & 0 \\ 0 & -r \end{pmatrix} \tag{A.4}$$

$$\mathbf{J}_{WP}(\phi) = \begin{pmatrix} 1 & 0 \\ 0 & \mathrm{e}^{-i\phi} \end{pmatrix} \tag{A.5}$$

For a half wave plate and a quarter wave plate is when for a particular wavelength, $\phi = \pi$ and $\phi = \pi/2$, respectively; the Jones' matrix results are $\mathbf{J}_{HWP}$ and $\mathbf{J}_{QWP}$.

$$\mathbf{J}_{WP}(\pi) = \mathbf{J}_{HWP} = \begin{pmatrix} 1 & 0 \\ 0 & -1 \end{pmatrix} \tag{A.6}$$

$$\mathbf{J}_{WP}\left(\frac{\pi}{2}\right) = \mathbf{J}_{QWP} = \begin{pmatrix} 1 & 0 \\ 0 & -i \end{pmatrix} \tag{A.7}$$

For an element that is rotated and angle, θ, along the optical axis, the Jones matrix, **J** is given by, (A.8).

$$\mathbf{J}(\theta) = \mathbf{J}_{ROT}(-\theta) \cdot \mathbf{J} \cdot \mathbf{J}_{ROT}(\theta) \tag{A.8}$$

These matrices represent a type of an optical element that when the electrical-wave interacts with; for the initial wave the electrical field is $\mathbf{E}_i$ the final after interacting is, $\mathbf{E}_f = \mathbf{J} \cdot \mathbf{E}_i$ For a polarizing beam splitter there will be two cases, when the beam reflects and when the beam transmits, that can be seen as a linear vertical and horizontal, respectively. Let's calculate the polarization state for the set up. Output of the laser y linear polarized but at an unknown angle.

$$\mathbf{J}_{Reference} = \mathbf{J}_{QWP}(-\beta) \cdot \mathbf{J}_M \cdot \mathbf{J}_{QWP}(\beta) \cdot \mathbf{J}_{LVP} \cdot \mathbf{J}_{HWP}(\alpha) \tag{A.9}$$

$$\mathbf{J}_{Sample} = \mathbf{J}_{QWP}(-\beta) \cdot \mathbf{J}_R \cdot \mathbf{J}_{QWP}(\beta) \cdot \mathbf{J}_{LHP} \cdot \mathbf{J}_{HWP}(\alpha) \tag{A.10}$$

For the quarter wave plate, the orientation will be set to be, $\beta = \pi/4$, to convert from a linear polarization state to a circular, at both arms. Solving the equation above we got , (A.11) and (A.12); from this equation we can note that when interacting again with the cube, first for the transmission case is $\mathbf{J}_{LHP} \cdot \mathbf{J}_{Reference} = \mathbf{J}_{Reference}$ and $\mathbf{J}_{LHP} \cdot \mathbf{J}_{Sample} = 0_{2,2}$, and for the reflection case we obtain that $\mathbf{J}_{LVP} \cdot \mathbf{J}_{Sample} = \mathbf{J}_{Sample}$ and $\mathbf{J}_{LVP} \cdot \mathbf{J}_{Reference} = 0_{2,2}$. From this, it is possible to conclude that for any initial polarization state, the beams and the reference arm will transmit and the sample will reflect in their return, that superposes each other in the out put of the interferometer, with linear orthogonal polarization state with each other.

$$\mathbf{J}_{Reference} = \begin{pmatrix} \sin(2\alpha) & -\cos(2\alpha) \\ 0 & 0 \end{pmatrix} \tag{A.11}$$

$$\mathbf{J}_{Sample} = \begin{pmatrix} 0 & 0 \\ -r\cos(2\alpha) & -r\sin(2\alpha) \end{pmatrix} \tag{A.12}$$

Let's name an electric field of the output beam, **E**, the output waves are then $\mathbf{E}_{Referrence} = \mathbf{J}_{Reference} \cdot \mathbf{E}$and $\mathbf{E}_{Sample} = \mathbf{J}_{Sample} \cdot \mathbf{E}$and if we calculate the interference term, I_{12}, which is the complex version for the calculation of the irradiance, and since $\mathbf{E}_{Referrence} \perp \mathbf{E}_{Referrence}$,

$I_{12} = 0$ meaning that there is no interference that is why in the set up shown at the figure, 3.2 after the interferometer, it is put an analyzer, which is a polarizer with free axis rotation, (A.14), for this case the angle will be fixed of $\pi/4$ in order get the equation, (A.15),

$$I_{12} \propto \left\langle \mathbf{E}^{\dagger}_{Reference} \cdot \mathbf{E}_{Sample} \right\rangle + \left\langle \mathbf{E}^{\dagger}_{Sample} \cdot \mathbf{E}_{Reference} \right\rangle \tag{A.13}$$

$$\mathbf{J}_{LHP}(\theta) = \begin{pmatrix} (\cos(\theta))^2 & \cos(\theta)\sin(\theta) \\ \cos(\theta)\sin(\theta) & (\sin(\theta))^2 \end{pmatrix} \tag{A.14}$$

$$\mathbf{J}_{LHP}\left(\frac{\pi}{4}\right) = \frac{1}{2}\begin{pmatrix} 1 & 1 \\ 1 & 1 \end{pmatrix} \tag{A.15}$$

Ignoring the beam splitter in the out that would not affect the polarization state, the Jones' matrix of the setup, $\mathbf{J}_{Setup}$ can be calculated with, (A.16), and it is shown at, (A.17).

$$\mathbf{J}_{Setup} = \mathbf{J}_{LHP}\left(\frac{\pi}{4}\right) \cdot \left(\mathbf{J}_{Reference} + \mathbf{J}_{Sample}\right) \tag{A.16}$$

$$\mathbf{J}_{Setup} = \frac{1}{2}\begin{pmatrix} \sin(2\alpha) - r\cos(2\alpha) & -\cos(2\alpha) - r\sin(2\alpha) \\ \sin(2\alpha) - r\cos(2\alpha) & -\cos(2\alpha) - r\sin(2\alpha) \end{pmatrix} \tag{A.17}$$

For a laser with a linear polarized at an angle, γ the electric field, $\mathbf{E}_{lp}$ can be written as is shown bellow,A.18. Let's apply $\mathbf{J}_{Setup}$, getting output field $\mathbf{E}_{out}$.

$$\mathbf{E}_{lp} = A\,\mathrm{e}^{i\phi}\begin{pmatrix} \cos(\gamma) \\ \sin(\gamma) \end{pmatrix} \tag{A.18}$$

$$\mathbf{E}_{out} = \mathbf{J}_{Setup} \cdot \mathbf{E}_{lp} \tag{A.19}$$

Leads to,

$$\mathbf{E}_{out} = \frac{1}{2}Ae^{i\phi}\begin{pmatrix} \sin(2\alpha-\gamma) - r\cos(2\alpha-\gamma) \\ \sin(2\alpha-\gamma) - r\cos(2\alpha-\gamma) \end{pmatrix} \tag{A.20}$$

For the calculation of the intensity we use the complex version as in, (A.13), $I \propto \left\langle \mathbf{E}^{\dagger} \cdot \mathbf{E} \right\rangle$, an the equation (A.21) is obtained, now using the Jones' matrix you loss the phase information of the wave, but what we want is that, (A.21) be in maximums. The localization of this will depend in the value of r, which strictly depends on the sample and the difference in the angles, $2\alpha - \gamma$; after some algebra it is possible to enrich to the solution for the maximum

intensity that is shown at equation, (A.22).

$$I \propto \frac{1}{2}A^2(\sin(2\alpha - \gamma) - r\cos(2\alpha - \gamma))^2 \tag{A.21}$$

$$2\,\alpha - \gamma = n\pi + \tan^{-1}\left(\frac{1}{r}\right), \qquad n \in \mathbb{Z} \tag{A.22}$$

Since, r will vary sample to sample and even point to during a scanning, is important to put in perspective this equation and to think at which angle you will work with.

International Master on
Control for Green Mechatronics

Title: Contribution to the characterization of elastic/mechanical displacements and quality factors of micron-scale mechanical/phononic resonators

Keywords: Optical Interferometry, Electro acoustic devices

Abstract:

The microelectro mechanical systems (MEMS) are an important contribution to the innovation of the technology that we use everyday, they are the core of mobile communication systems. The characterization of MEMS is needed to develop a better performance of the device, this is key but challenging because stringent conditions have to be fulfilled.

The objective of this research is to implement a homodyne Michelson interferometer that contributes to characterize the surface acoustic waves in MEMS and phononic devices. The main characteristic of the homodyne interferometer is that the waves that interfere have the same optical frequency. The implementation of a homodyne Michelson interferometer with two option of stabilization, using a feedback controller and a Quadrature detection approach has been explored.

The mechanical displacement of two devices were characterized, also the quality factor of one of them was obtained. It was achieved to implement a homodyne interferometer for the measurement of out of plane vibration. The functioning of the interferometer was proved from 100 Hz to 3 MHz. The amplitude limit was found to be $0.14pm/\sqrt{Hz}$. The frequency limit of this homodyne has an electronical limit of 1.2 GHz.

Université Bourgogne Franche-Comté
32, avenue de l'Observatoire
25000 BesanÃğon, France